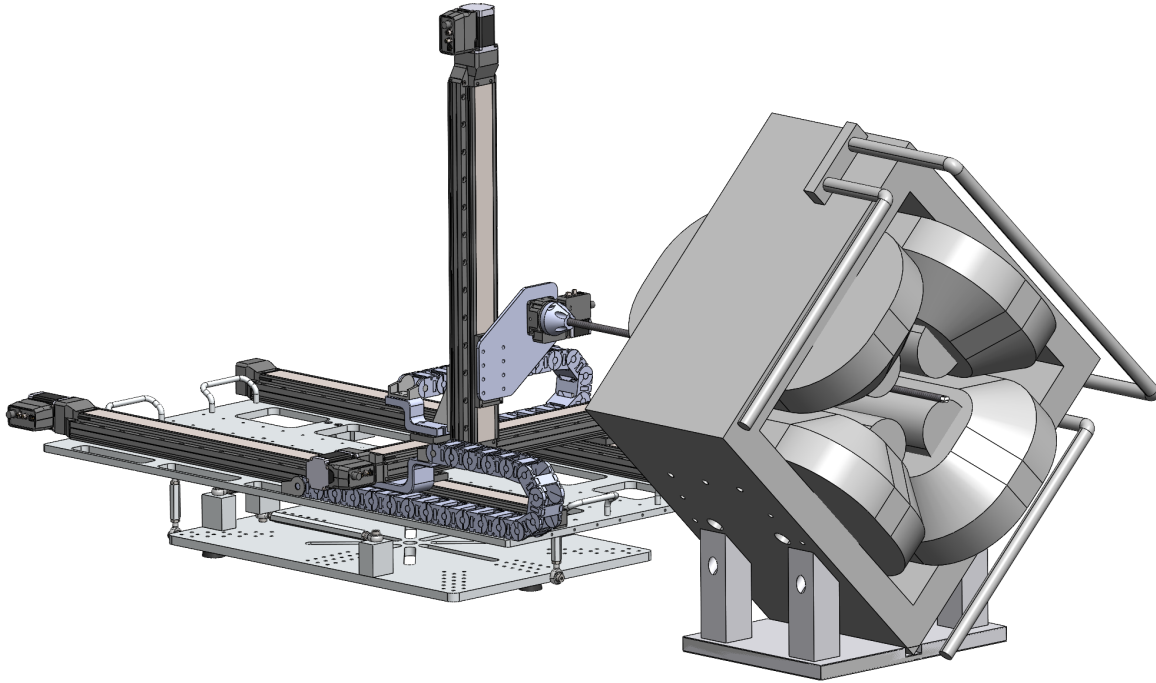


16T Magnet Mapper



Benjamin Brown

Andrew Kassab

Joshua Kraan

Alice Xiong

Project Sponsors:

Dr. Marco Marchetto

TRIUMF

Project 2204

Applied Science 459

Engineering Physics Project Laboratory

The University of British Columbia

April 8, 2022

1 Executive Summary

TRIUMF utilizes electromagnetics to control its beamlines. The magnetic fields of these electromagnetics must be well understood for efficient and safe control. Dr. Marco Marchetto commissioned a magnet mapping device (“the mapper”) capable of measuring the magnitude and direction of the magnetic fields produced by the beamline electromagnets. Over the past eight months, our team has developed this mapper.

We chose a three axis cartesian motion gantry with a rotational stage to map the transverse fields in quadrupoles and the vertical fields in dipole magnets. The mapper can map a region of 0.5 m x 0.5 m x 1.0 m, compatible with most magnets at TRIUMF and can capture fields down to 0.25" away from a magnet's surface. A carbon fiber boom isolates a MPT-141 hall probe from the motion system's motors during mapping. The boom's high specific stiffness minimizes the boom's mechanical damping time.

The time required for electronic and mechanical damping limits the mapper's ability to capture high resolution grids in a reasonable time frame. Currently, the probe's electrical settling time of 5 seconds is the largest contributor to the mapping duration. We performed a preliminary field mapping of a steerer magnet in 2.5 hours.

Due to misalignments in the vertical and rotation stages, the mapper's current accuracy is not sufficient to measure with a 1 mm grid spacing. However, if the angular offsets can be addressed, the system's accuracy will approach the expected linear accuracy of the motion system of 0.25 mm.

Despite these issues, we have performed mappings of magnets at TRIUMF with excellent agreement with simulated magnetic field values. We are confident the system can function as required by Dr. Marchetto. We suggest redesigning the adapter between the boom and the rotation stage, and shimming the vertical stage to improve the system's accuracy. On the software side, we recommend integrating the system's controller with EPICS and investigating packet loss. Upon validating the system's absolute positional and magnetic accuracy, the mapper will be ready to enter full-time service as an instrument at TRIUMF.

2 Table of Contents

1 Executive Summary	i
2 Table of Contents	ii
3 Table of Figures	iv
4 Introduction	1
4.1 TRIUMF	1
4.2 Background and Significance	1
4.3 Problem Statement	3
4.4 Scope and Limitations	3
5 Discussion	4
5.1 Theory	4
5.1.1 Electromagnets	4
5.2 Requirements	6
5.2.1 Measurement Volume	6
5.2.2 Timing	7
5.2.3 Alignment	8
5.2.4 Accuracy	9
5.2.5 Magnetic Interference	9
5.2.6 Budget	9
5.3 Design	10
5.3.1 Overview	10
5.3.2 MPT-141 Hall Probe	11
5.3.3 Probe Holder	12
5.3.4 Boom	15
5.3.5 Motion System	16
5.3.6 Rotation	18
5.3.7 Cable Management	20
5.3.8 Alignment	21
5.3.9 Probe Electrical Interface	23
5.3.10 Software System	23
5.4 Tests and Results	26
5.4.1 System Alignment	26
5.4.2 Boom Oscillation Testing	27
5.4.3 Magnetic Field Steerer Mapping	29
5.4.4 Quadrupole Magnet Mapping	30

6 Conclusion	32
7 Recommendations	33
8 Deliverables	35
9 Appendix A	36
9.1 Bill of Materials	36
9.2 Boom Optimization Calculations	38
9.3 Hall Effect Sensors	39
9.4 Accuracy and Repeatability	40
9.5 System Alignment Report	41
9.6 Motion System Comparison	42
9.7 Mapper Assembly Views	44
9.8 Acknowledgements	46
10 Appendix B: User Manuals	47
10.1 Probe Holder Installation	47
10.2 Zaber Launcher User Guide	49
10.3 Mapper Control Software User Guide	52
11 References	58

3 Table of Figures

- Figure 1. Quadrupole magnets and their fields
- Figure 2. Dipole magnet and its field
- Figure 3. Quadrupole and dipole magnets used at TRIUMF
- Figure 4. Overview of magnet mapper problem
- Figure 5. Electromagnetic field lines due to current through a coil
- Figure 6. 16T dipole magnets at TRIUMF
- Figure 7. Quadrupole magnets installed at TRIUMF and their magnetic
- Figure 8. Measurement volume for a quadrupole magnet
- Figure 9. Maximum probe and boom diameter
- Figure 10. Measurement time vs. grid spacing.
- Figure 11. Axis misalignments
- Figure 12. Measurement grids illustrating accuracy and repeatability
- Figure 13. Magnet mapper system diagram
- Figure 14. MPT-141 hall probe
- Figure 15. MPT-141 hall probe holder (original)
- Figure 16. Hall probe holder and reference surface
- Figure 17. Section view of the probe holder assembly
- Figure 18. The top and bottom pieces of the probe holder
- Figure 19. Acceleration perpendicular to the boom axis
- Figure 20. The X-LRT motion system
- Figure 21. Rotation system diagram
- Figure 22. Rotation stage to boom adapter
- Figure 23. Cross section of rotation stage to boom adapter
- Figure 24. Cable routing and cable chains
- Figure 25. Probe cable torsion relief
- Figure 26. Turnbuckle alignment table
- Figure 27. Coordinate measurement machine (CMM) at TRIUMF
- Figure 28. Teslameter connections and switches
- Figure 29. Software system flowchart
- Figure 30. Mapper coordinate system
- Figure 31. Terminal interface for setting configurations

- Figure 32. Sample path and path edges
- Figure 33. Time domain accelerometer data from oscillation testing
- Figure 34. Frequency domain accelerometer data from oscillation testing
- Figure 35. Field mapping setup
- Figure 36. Mapper readings and simulated field strength
- Figure 37. Quadrupole magnet mapping setup
- Figure 38. Quadrupole mapping results
- Figure 39. Hall probe diagram
- Figure 40. Accuracy and repeatability.
- Figure 41. Alignment report axis labels
- Figure 42. Alignment report results
- Figure 43. LRT and LC40 motion systems
- Figure 44. Mapper assembly front view.
- Figure 45. Mapper assembly side view.
- Figure 46. Mapper assembly isometric view.
- Figure 47. Mapper assembly top view.
- Figure 48. Basic movement window
- Figure 49. Checking the COMM port and X,Y,Z offsets
- Figure 50. Moving the linear stages in Zaber Launcher
- Figure 51. Checking rotation and moving the rotation stage
- Figure 52. Close the serial port in Zaber Launcher
- Figure 53. Starting the control software
- Figure 54. Identifying the profile in the configuration file.
- Figure 55. Main menu of mapper control software
- Figure 56. Configurations common to all motion shapes (I)
- Figure 57. Configurations common to all motion shapes (II)
- Figure 58. Configurations specific to rectangular motion shape
- Figure 59. Configurations specific to cylinder motion shape
- Figure 60. Configurations specific to custom motion shape
- Figure 61. Changing the ‘z_range’ configuration.
- Figure 62. Confirming settings, saving, and generating path CSV.
- Figure 63. Main menu of mapper control software

4 Introduction

4.1 TRIUMF

Our capstone is sponsored by Dr. Marco Marchetto, the leader of the Engineering Physics group at TRIUMF — the largest particle accelerator center in Canada. Scientists at TRIUMF use electromagnets to manipulate and direct particles at high velocities, advancing fundamental research and producing medical isotopes for non-invasive treatments.

4.2 Background and Significance

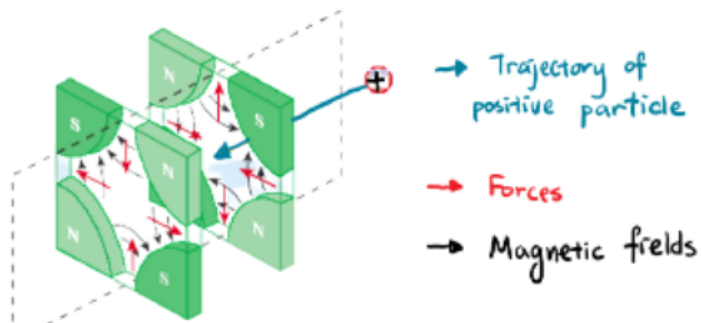


Figure 1. Quadrupole magnets and their fields (Magnetic Multipoles, n.d.).

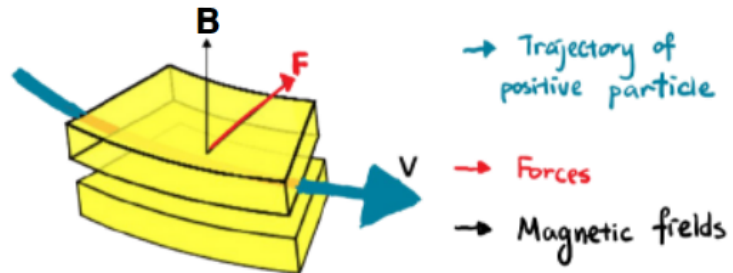
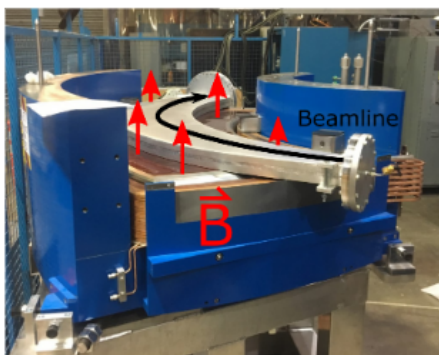


Figure 2. Dipole magnet and its field (How Do Synchrotrons Work?, 1997).

Electromagnets apply a Lorentz force on charged moving particles. Quadrupole magnets create an overall field that focuses the beam. Dipole magnets can bend the particles and separate different masses. Together, arrays of electromagnets can manipulate particle beams along different trajectories and lead to interesting experiments.

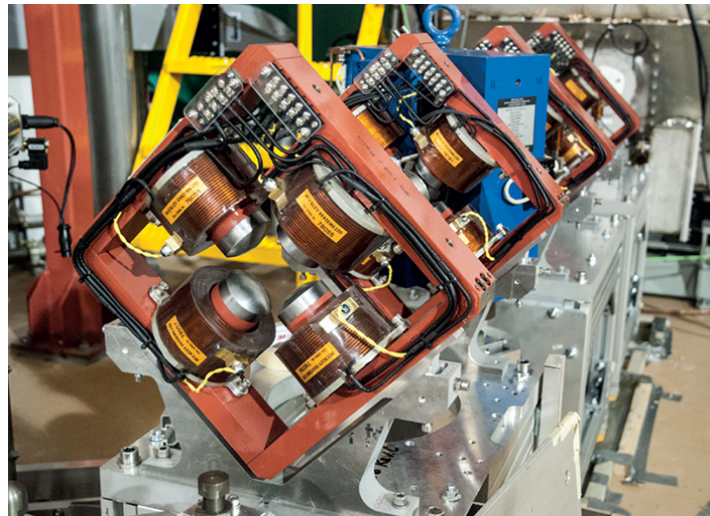


Figure 3. Quadrupole magnets (red) and dipole magnets (blue) used at TRIUMF (ARIEL Begins a New Future in Rare Isotopes – CERN Courier, 2015).

Due to fringe fields, material impurities, and manufacturing imperfections, magnets have non-uniform behaviours that cannot be predicted by simulations. Hence, scientists at TRIUMF need to collect data from each magnet, compare it to their models, and make corrections accordingly.

Our magnet mapper provides scientists with an instrument to systematically perform field measurements allowing for finer controls, safer operations, and reduced experimental uncertainties.

4.3 Problem Statement



Figure 4. Overview of magnet mapper problem.

The high level goal of the magnet mapper is to automate the collection of magnetic field data from user-defined points with a minimum grid resolution of 1 mm. We needed a modular design compatible with different sensors and both dipole and quadrupole magnet shapes (bounded by a 1 m x 0.5 m x 0.5 m box). Distancing all magnetic components on the mapper is necessary to avoid interfering with measurement. The mapper should spend no more than a day per magnet measurement, given a grid resolution around 20 mm. The mapper should also tabulate position and magnetic field vectors after each measurement.

4.4 Scope and Limitations

At Dr. Marchetto's request, our project aims at developing a minimum viable product so TRIUMF can start using the magnet mapper immediately, with potential for future upgrades. TRIUMF provided us with a uniaxial hall probe and associated teslameter to measure fields.

TRIUMF experts will fabricate a turnbuckle table and precisely align the mapper to the magnets. The user interface is limited to the command line. Integration with Experimental Physics and Industrial Control System (EPICS) and a graphical interface are reserved for future updates.

5 Discussion

We will first discuss the basic theory of electromagnets to provide context for the project requirements and discussion.

5.1 Theory

5.1.1 Electromagnets

Electromagnets are devices capable of producing strong magnetic fields — a prerequisite for beamline control. By inducing current in a coil, a magnetic field is generated.

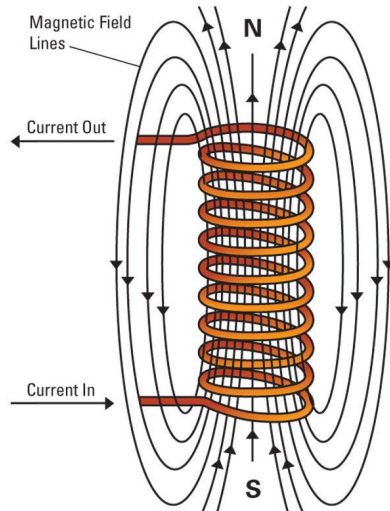


Figure 5. Electromagnetic field lines due to current through a coil (Electromagnets, n.d.).

Dipole magnets are used as mass separators at TRIUMF. Their fields, shown in **Figure 6**, are oriented vertically, so our mapper only needs to measure the field strength in one direction.

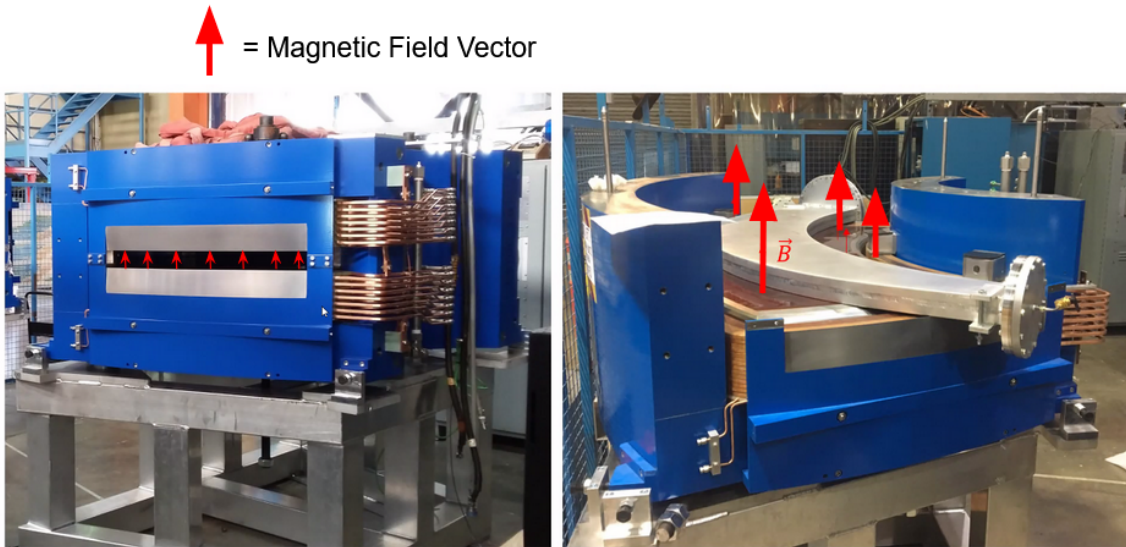


Figure 6. Dipole magnets: (left) an assembled 16 tonne dipole magnet, (right) identical magnet with top half removed. (Marchetto, 2021).

Quadrupole magnets (**Figure 7**) function as magnetic lenses. We need to measure the X, Y components of the magnetic field to characterize their interactions with beamline particles.

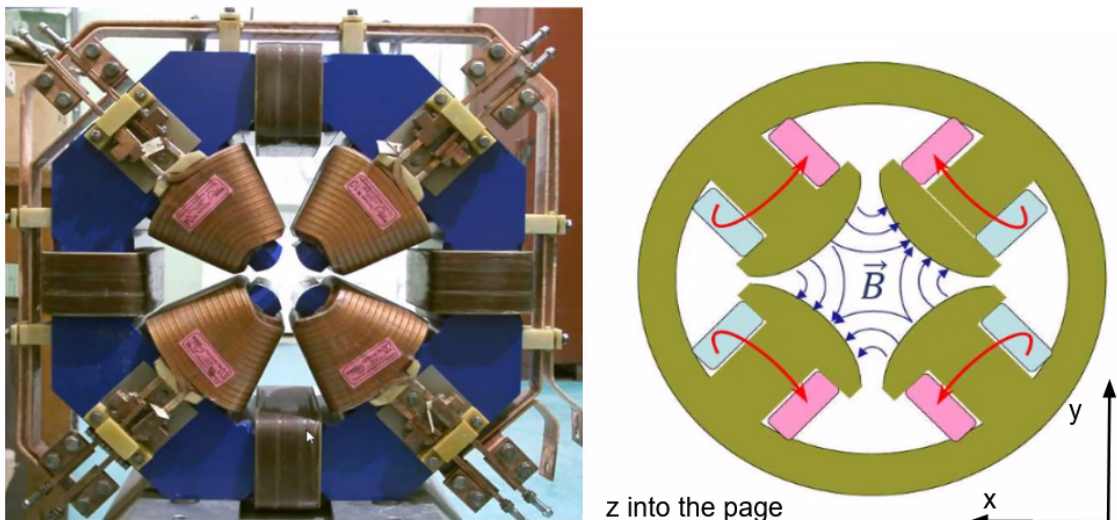


Figure 7. Quadrupole magnets: (left) Quadrupole magnet installed at TRIUMF, (right) magnetic field diagram for a quadrupole. Current circulation direction indicated in red. Beamline particles travel along the z axis. (Marchetto, 2021).

The Z component of the field exerts no force on the beamline, as can be determined from the Lorentz force equation for magnetic fields below. This component is ignored during mapping.

$$\vec{F} = q\vec{v} \times \vec{B}$$

5.2 Requirements

The physicists at TRIUMF provided the requirements (**Section 4.3**) on their end, then we translated those requirements into the engineering constraints that drove our design.

5.2.1 Measurement Volume

We sized our mapper to be capable of mapping the largest magnet at TRIUMF, a 16 tonne dipole. This results in a traversal distance of 0.5 m x 0.5 m x 1 m. An example of a measurement volume is shown below in **Figure 8**. In order to take measurements 0.25" from the magnet surfaces, as required by the physicists, the outer diameter of the boom and probe must be kept under 0.5", as demonstrated in **Figure 9**.

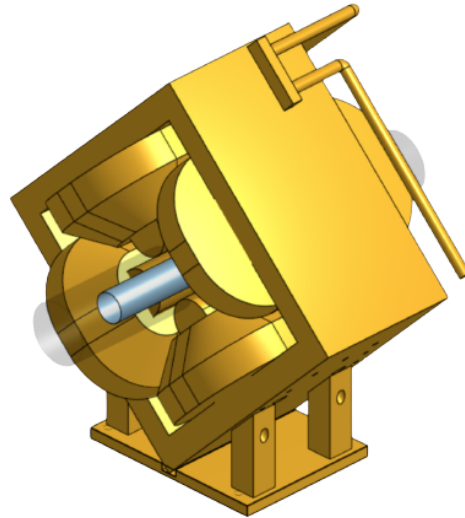


Figure 8. Measurement Volume for a Quadrupole Magnet.

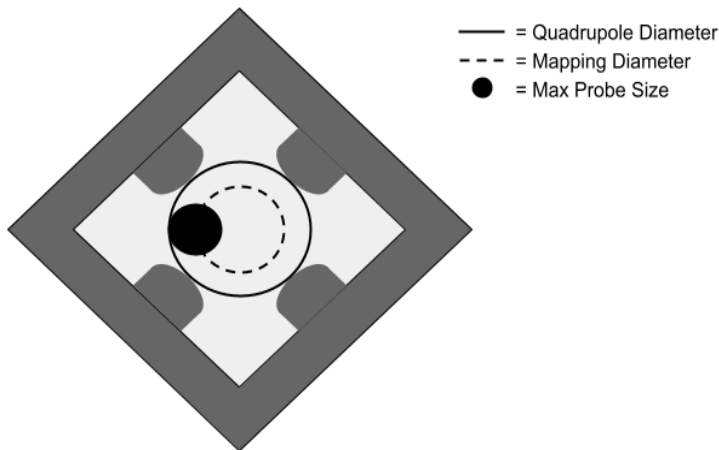


Figure 9. Maximum Probe and Boom Diameter to Avoid the Surface of the Magnet.

5.2.2 Timing

The number of points measured significantly influences the mapping time as seen in **Figure 10**. The mapper should measure all relevant magnets at a relevant grid spacing within a few days.

Measurement Time vs Grid Spacing

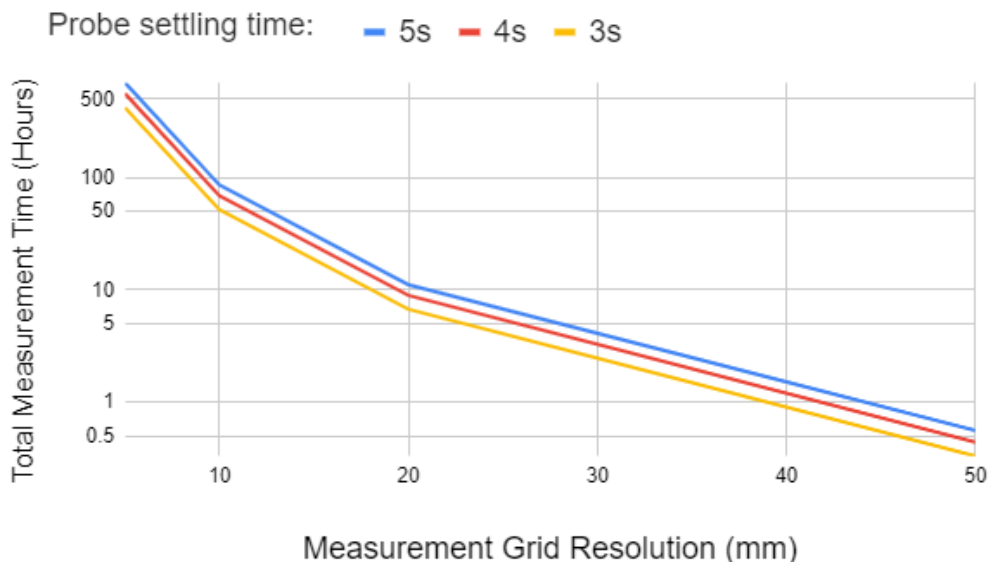


Figure 10. Measurement Time (Log Scale) vs. Grid Spacing. This plot assumes measurement on a cylinder of 100 mm diameter and 1000 mm side length.

5.2.3 Alignment

The probe location must be very well known with respect to the magnet when taking a measurement. As a result, the mapper axes must be very accurately aligned with the magnet axes. Translational offsets can be corrected in software, but angular misalignment cannot (see **Figure 11**), so angular misalignment must be minimized before the measurement.

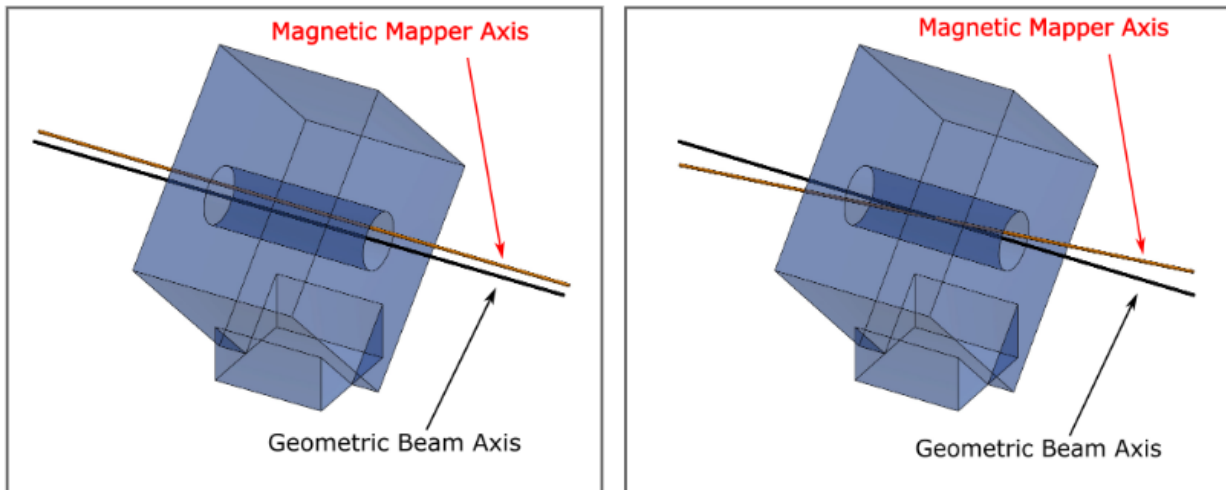


Figure 11. Axis misalignments: (left) Translational offset which can be corrected in software. (right) Angular misalignment between the mapper and magnet axes which cause incorrect field components to be measured. Angular misalignment cannot be corrected in software.

5.2.4 Accuracy

Dr. Marchetto requires a mapper capable of a 1 mm measurement grid spacing. We derived the required accuracy of the motion system, as defined in **Appendix 9.4**, from this requirement. As seen in **Figure 12**, we require an accuracy of at least 0.5 mm to faithfully measure a 1 mm grid.

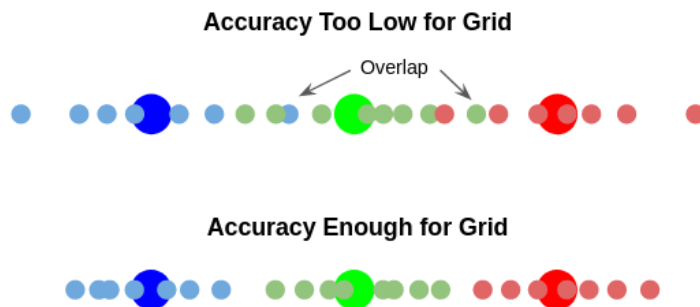


Figure 12. Measurement grids: The commanded positions are indicated by large dots and the actual positions of the motion system are indicated by smaller dots of the same color. If the accuracy is less than half the grid spacing, then a commanded measurement may not correspond to the correct location.

5.2.5 Magnetic Interference

We need to minimize interference from magnetic components on the mapper to ensure accurate measurements. We require an approximate minimum distance of 0.5 m between the magnet and any ferromagnetic materials or moving electrical conductors. Testing will be required to ensure any interference is negligible.

5.2.6 Budget

Dr. Marchetto indicated a preference for a system around ten to twenty thousand Canadian dollars.

5.3 Design

5.3.1 Overview

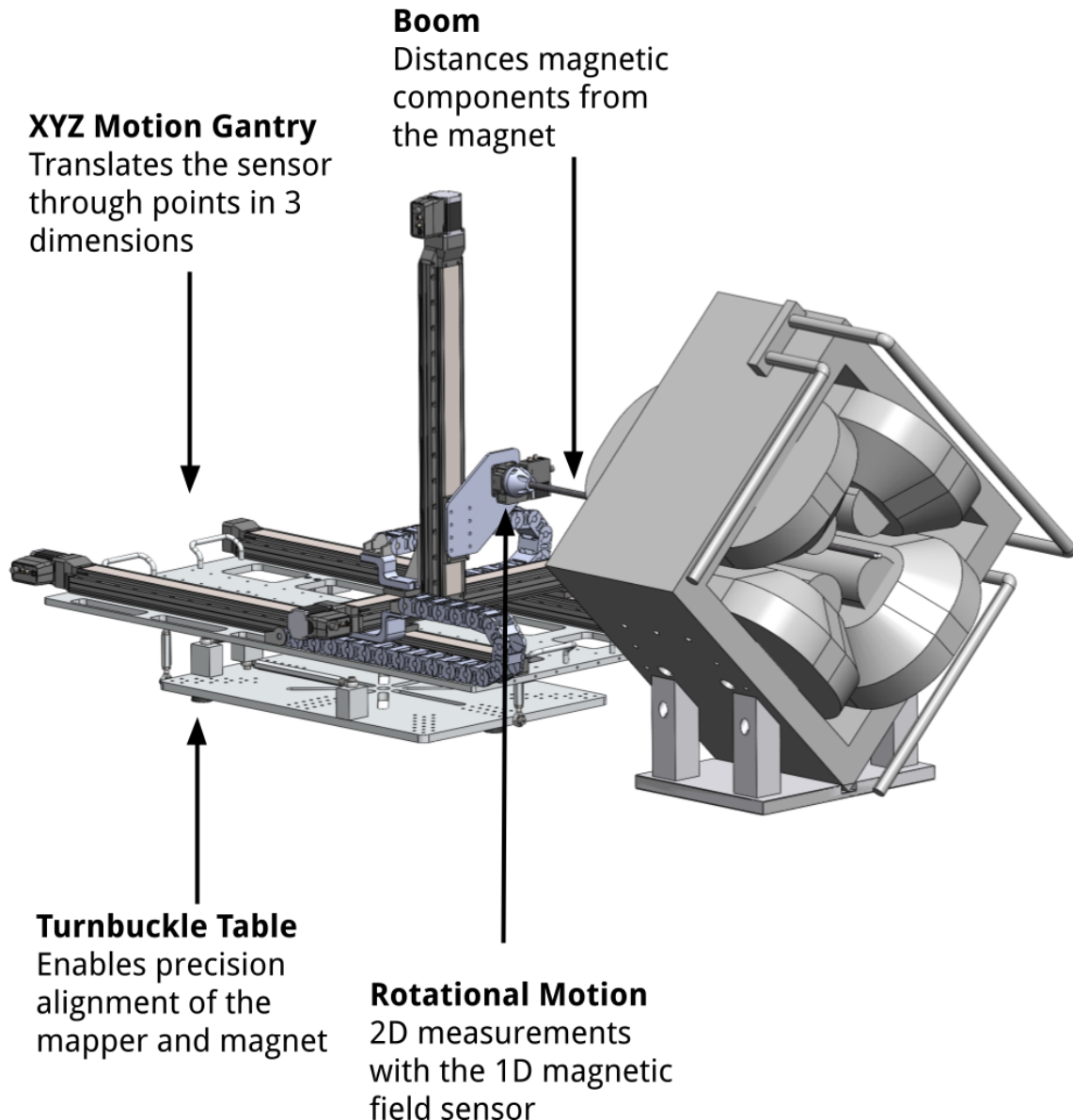


Figure 13. Magnet mapper system diagram.

We settled on a 4-axis motion gantry with the hall probe mounted at the end of a non-ferromagnetic boom. This section will outline the system while later sections will dive deeper into the details of each subsystem.

Boom

The magnetic field sensor is mounted to the end of a carbon fiber boom which distances magnetic components from the magnet. The boom is interchangeable for different lengths.

Rotation

Some of the magnets have 2D magnetic fields so we must rotate the uniaxial probe to capture these fields. A rotation stage from Zaber is mounted to the end of our 3-axis gantry allowing for ± 180 degrees of rotation.

XYZ Motion Gantry

In addition to rotating the probe, we translate it in 3 cartesian directions using a Zaber 3-axis motion gantry which provides accurate and robust control. A centralized software controller interfaces with all of the built-in motor controllers.

Turnbuckle Table

TRIUMF's standard high precision turnbuckle system allows for fine tuning of the mapper with 6 degrees of freedom. As such, the mapper and magnet can be precisely aligned before turning the mapper on.

5.3.2 MPT-141 Hall Probe

TRIUMF supplied our team with a Group3 MPT-141 uniaxial hall probe, a diagram of which can be seen in **Figure 14**.

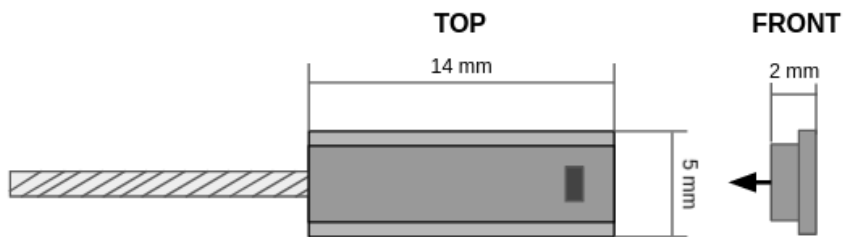


Figure 14. MPT-141 hall probe. The sensing element is indicated by a grey box. The probe is uniaxial, meaning it only measures the magnetic field in the direction indicated by the arrow. More information and detailed drawings are available on Group3's website (Aguas, 2018).

The probe is connected to a 12 m, 8-conductor shielded coaxial cable to deliver the analog magnetic field measurement to the provided DTM-151 teslameter. Once interpreted by the teslameter, the reading is converted to a digital signal.

The cable of the probe has 3 sections: a short bare section, a longer insulated section, and a shielded section, which makes up the majority of its length. The bare and insulated sections can be seen in **Figure 15**.



Figure 15. MPT-141 hall probe mounted in an aluminum probe holder. The holder shown was too large and heavy to be used.

5.3.3 Probe Holder

The probe holder must allow the hall probe to be attached and removed from the mapper, ensure the measurement direction is perpendicular to the boom axis, fix the probe rotationally and longitudinally relative to the boom, and protect the probe and its delicate cable.

As the probe holder enters magnets, from the requirements stated in **Section 5.2**, it must be nonmagnetic and a maximum diameter of 0.5". The holder is mounted inside the boom, which has an inside diameter of 0.375".

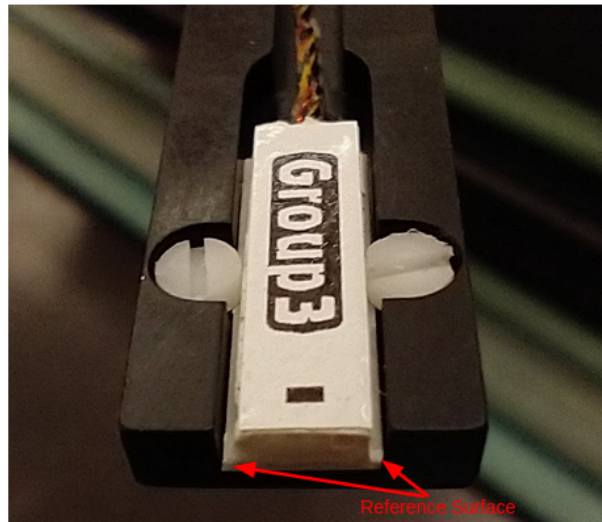


Figure 16. Hall probe mounted in aluminum holder, with reference surface indicated.

Fasteners could not be used for the new probe holder as the screw heads would intersect the boom. We settled on a 3D printed probe holder that uses compliant material to hold the probe and the holder in place. The holder was printed on a Formlabs Form 3 Stereolithography (SLA) printer to produce features as small as 0.3 mm.

A view of the probe holder assembly with parts of the boom and holder sectioned is shown in **Figure 17**, and the top and bottom pieces of the holder are shown in **Figure 18**.

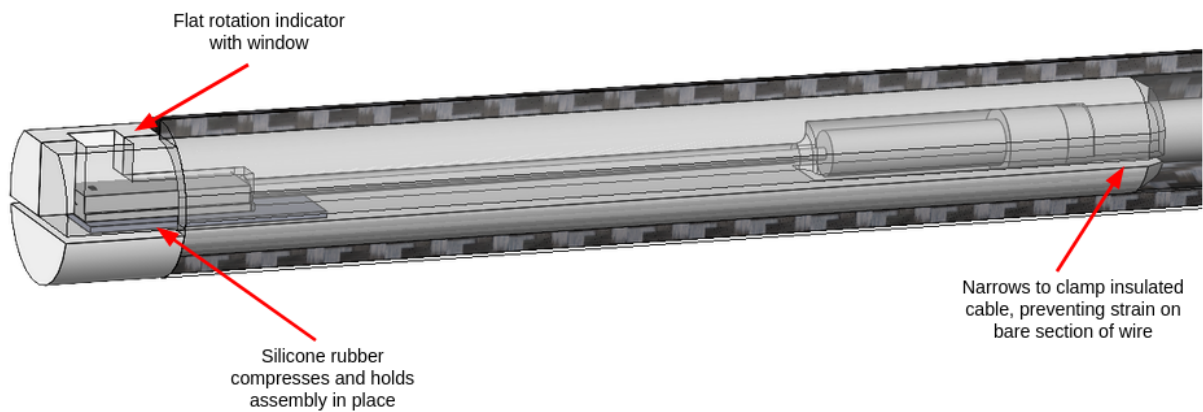


Figure 17. Section view of the probe holder assembly mounted in the boom.

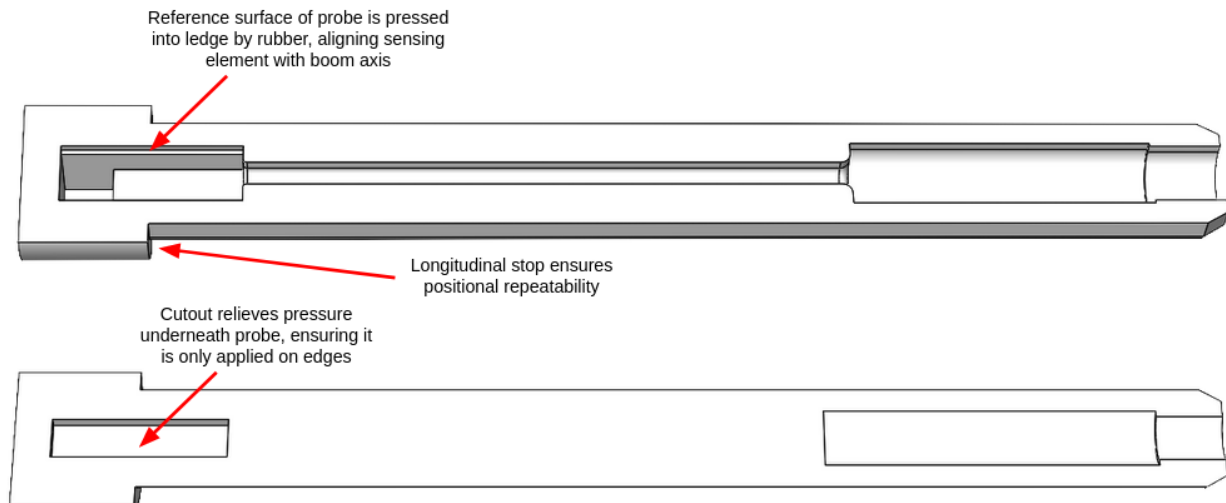


Figure 18. The top and bottom pieces of the probe holder.

A piece of silicone rubber underneath the probe and the insulation on the probe cable are both compressed so they firmly seat the holder against the inner wall of the boom when installed to prevent motion during operation. The amount of compression of the rubber was tuned by modifying the thickness of the bottom piece until the holder sat firmly in the boom without being too difficult to remove.

The flat section on the top holder allows the direction of the measurement axis to be externally measured. To determine the probe's position relative to the motion system, we recommend that TRIUMF use their laser profiler to characterize the top piece of the holder. The hall probe seat was initially sized based on the maximum of the tolerances reported by Group3; however, we found that the length was approximately 0.2 mm larger than specified.

Instructions for installing the hall probe into the probe holder are included in **Appendix 10.1**.

5.3.4 Boom

The boom distances the hall probe from the magnetic components of the mapper.

The boom will enter the magnet during measurements, so it must be non-magnetic and have a maximum outer diameter of 0.5". To utilize the full range of motion, a 1 m boom is required.

Boom oscillation was a design concern as it increases measurement time. **Figure 19** shows how boom acceleration can induce oscillation.

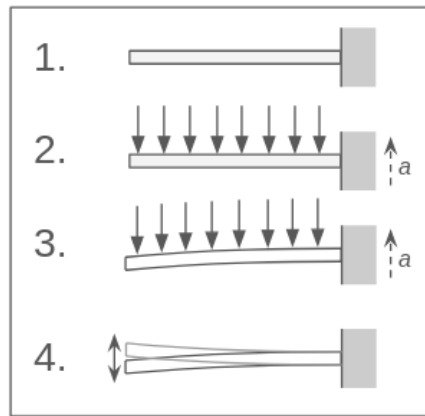


Figure 19. Acceleration perpendicular to the boom axis causing bending and oscillation.

Appendix 9.2 details the calculations done to optimize the boom's material and shape. We found that a higher natural frequency minimizes the oscillation time. This is achieved by a boom with a high specific stiffness and a thin wall, as indicated by the following proportionality:

$$f_1 \propto \sqrt{\frac{E}{\rho} (r_o^2 + r_i^2)}$$

E = Young's Modulus (Pa)

ρ = Density (kg/m^3)

r_o = Outer Radius (m)

r_i = Inner Radius (m)

Here we assume a fixed boom length; a shorter boom significantly increases the natural frequency as:

$$f_i \propto 1/L^2$$

We designed the booms to be easily exchangeable, so that a shorter boom could be installed for faster damping.

We chose a 1/16" wall thickness carbon fiber boom, a very high specific stiffness material. We estimated that the natural frequency for a 1 m long boom would be 22 Hz; however, the added mass of the probe holder and the probe cable lowered the actual value (see **Section 5.4.2**).

5.3.5 Motion System

The motion system must be able to accurately move the hall probe to thousands of locations within the measurement volume.

From **Section 5.2**, the desired measurement volume is 0.5 m x 0.5 m x 1.0 m, and the required linear positional accuracy is 0.5 mm. High reliability and ease of maintenance were key requirements for this system, so we prioritized a commercial motion system from a reliable company over a custom-made one.

A cartesian linear motion system with probe rotation was chosen as it was best able to adapt to the relevant magnet types, and was the simplest to implement.

At TRIUMF's recommendation, we primarily focused on offerings from Zaber Technologies. The budget and accuracy requirements narrowed the range of suitable motion systems to two, which are compared in **Appendix 9.6**. Due to its better linear positional accuracy specification of 0.25 mm and a higher estimated natural frequency, we recommended the X-LRT system shown in **Figure 20**.

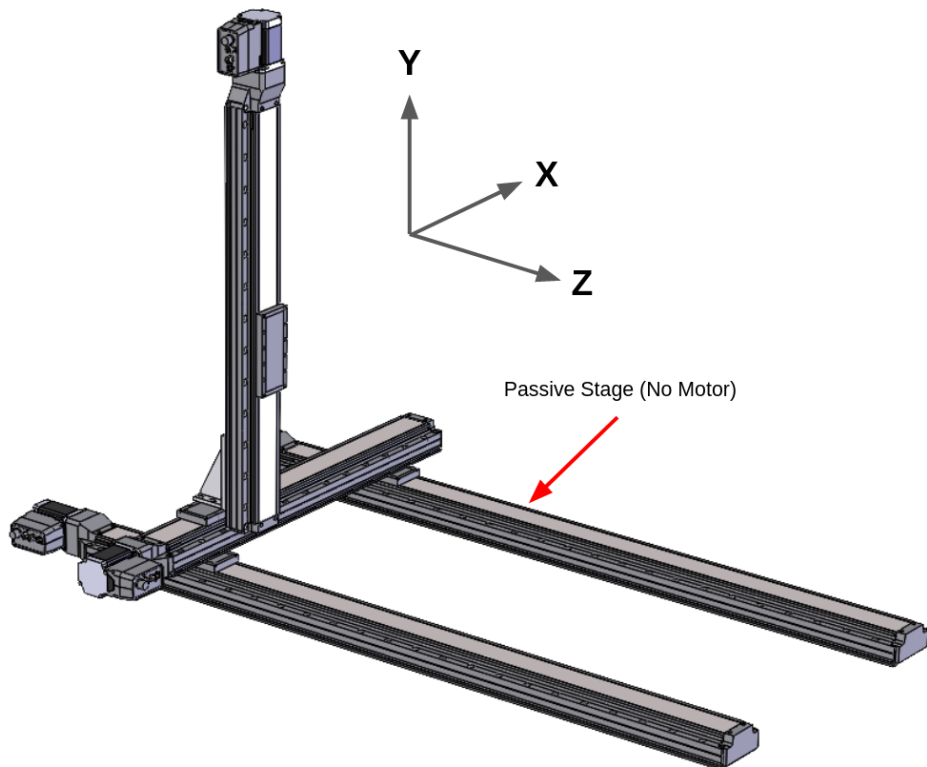


Figure 20. The X-LRT motion system, with axis convention indicated. An additional passive bottom stage prevents bending during motion along the X axis.

For the X-LRT system, we specified built-in controllers to enable power and signal to be shared between each linear stage with a single cable. We specified the leadscrew pitch and the power supply for continuous operation at light loads based on Zaber's recommendations. Linear encoders were outside the budget of the project, but we considered rotary encoders, which do not directly measure stage position, but can detect when motor rotation does not match what was commanded. After discussion with a Zaber specialist, we determined that this was typically caused by high loads that were unlikely for this application, so we decided against purchasing them.

During testing, we noticed the motion system appeared to lose track of its position when left stationary and powered on overnight. This could be a drawback of the fully open loop control that was chosen, but the cause is not yet clear.

5.3.6 Rotation

When mapping quadrupoles, we must measure the two transverse magnetic field components (**Section 5.1.1**). This measurement is achieved by rotating our uniaxial probe by 90° at every measurement location. The rotations system sits between the vertical gantry and the boom (**Figure 21**).

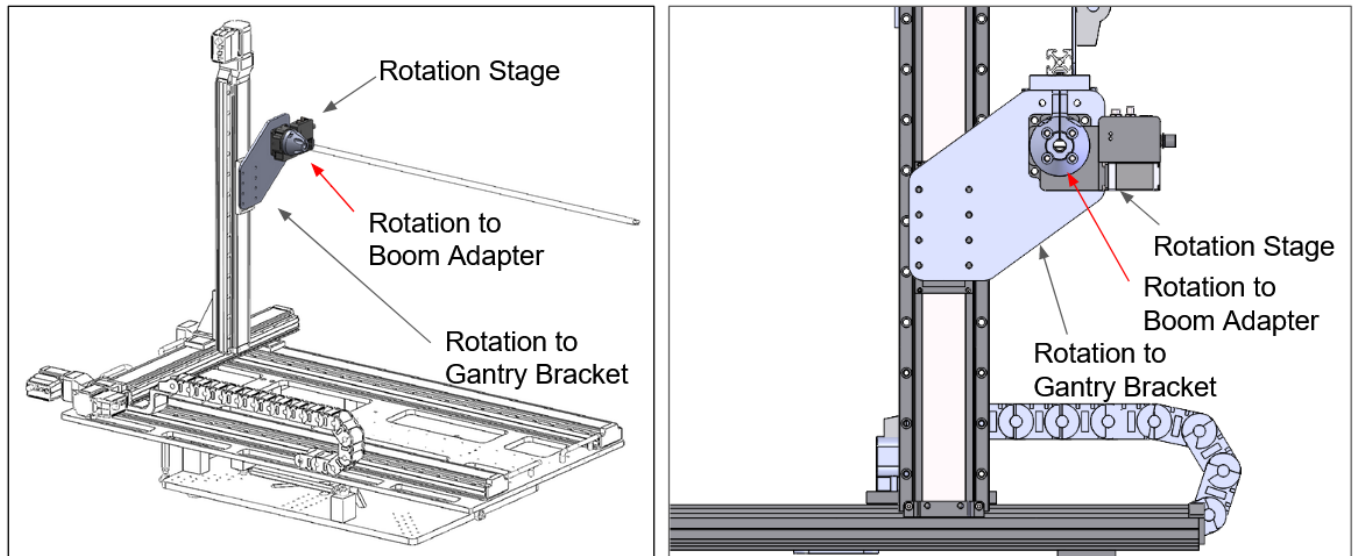


Figure 21. Rotation System Diagram: (left) the rotation system sits between the vertical gantry and the rotation system; (right) view of the rotation system with the boom out of the page. The Rotation to Gantry Bracket provides clearance to the probe cable as it exits the boom. The Rotation Stage rotates the boom. The Rotation to Boom Adapter connects the rotation stage with the boom.

We used a Zaber rotation stage as they are reliable and compatible with the motion system's controllers. The boom to rotation stage adapter (**Figure 22** and **Figure 23**) incorporates ID (Inner Diameter) and OD (Outer Diameter) guide features to ensure the boom and rotation stage axes are aligned.

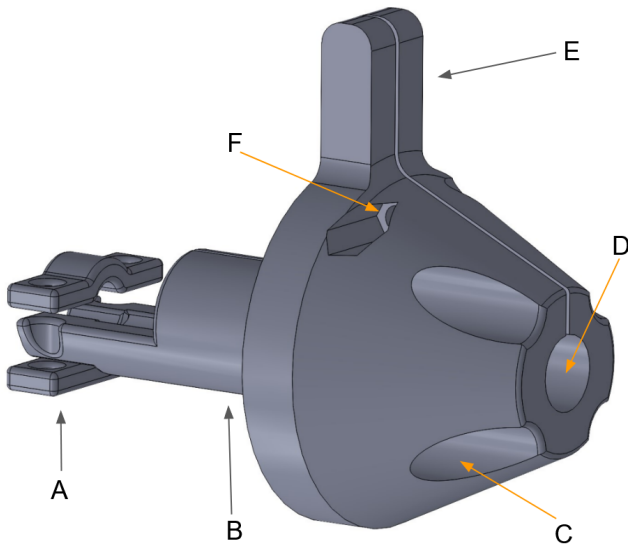


Figure 22. Rotation stage to boom adapter. (A) Probe cable clamp prevents the probe cable from rotating inside the boom. (B) OD guide feature interfacing with the rotation stage. (C) Bolt holes for attaching to the rotation stage. (D) ID guide feature interfacing with the boom. (E) Hardstop to prevent over-rotation. (F) Captured nut to apply clamping pressure to the boom.

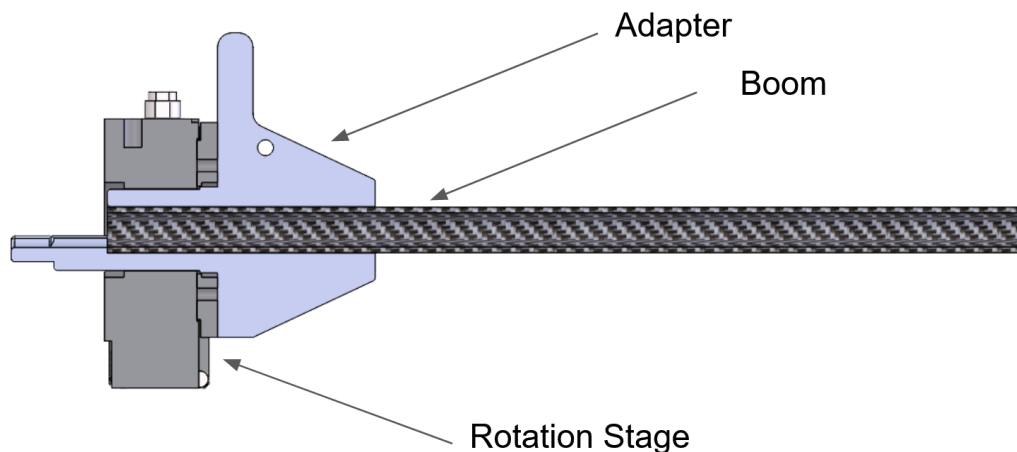


Figure 23. Cross section of rotation stage to boom adapter. The concentricity of the boom and the rotation stage is determined by the dimensional accuracy of the OD and ID guide features.

The adapter was FDM printed and, as discussed in **Section 5.4.4**, introduced an angular misalignment between the rotation stage axis and the boom axis. We recommend reprinting this component with a higher accuracy printer or designing a machined component to resolve this issue.

5.3.7 Cable Management

Power and movement commands must be delivered to the four Zaber stages via cables. A single cable runs between each stage, as power and control signals are daisy chained (Moreno, 2017). The hall probe's cable must also be routed from the probe to a digital teslameter.

We used cable chains to house the cables travelling between the linear motion stages to prevent the cables from kinking or getting pinched during motion. The chain's bend radius was chosen to exceed the minimum bend radius of our cables. We mounted the chains to the mapper with custom 3D printed brackets (**Figure 24**).

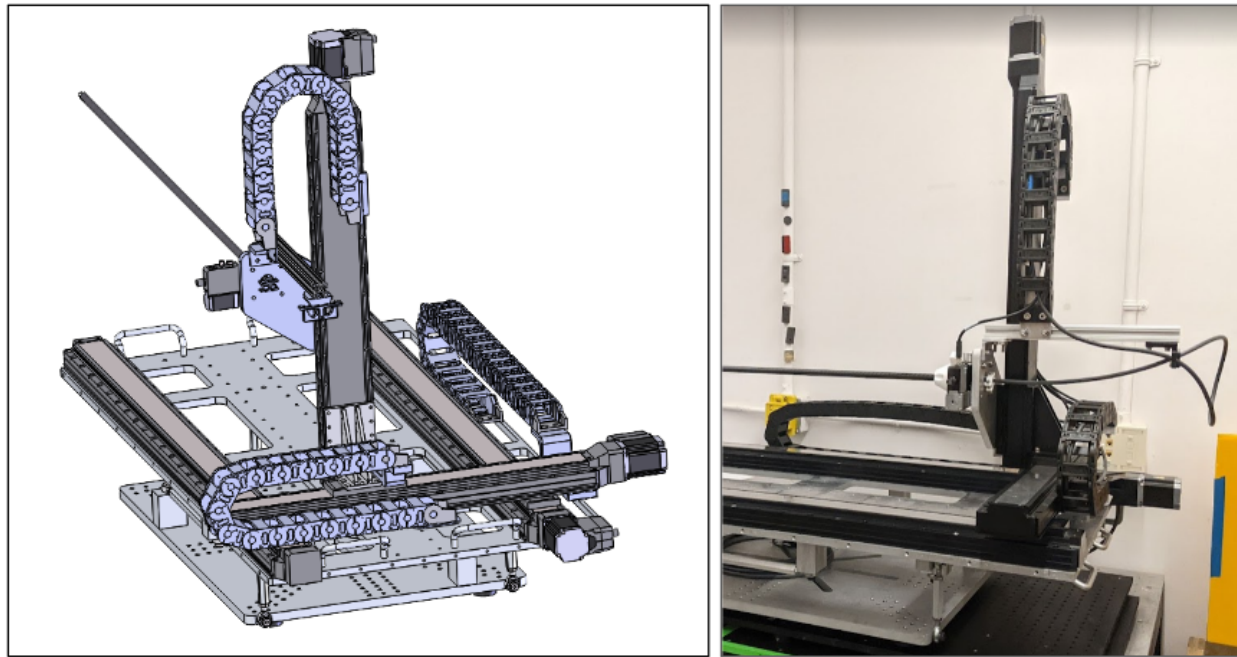


Figure 24. (left) A cable chain protects the cables on each linear stage. Cables are rigidly mounted to the mapper body or inside the cable chains to avoid wear. (right) Motion control and power cables for the four Zaber stages and the probe cable are routed through the cable chains.

The rotational stage required additional cable management to prevent torsional strain from shearing the cable as we rotated the cable as shown (**Figure 25**).

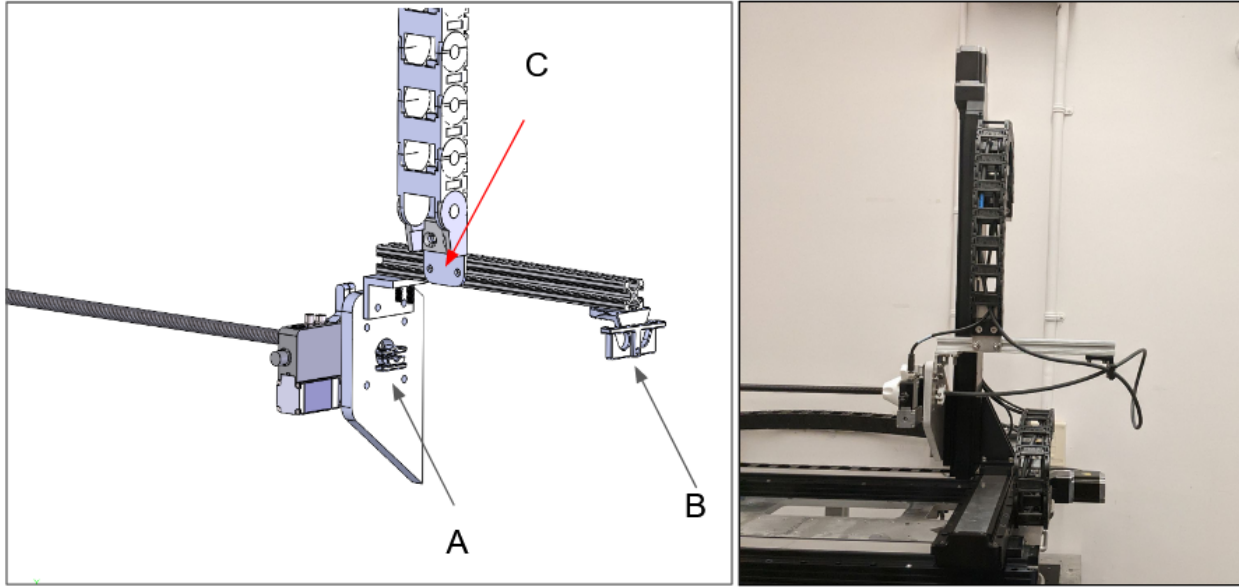


Figure 25. (left) The probe cable is rigidly mounted to boom at A and mounted to the motion system at C. Unsupported distance from A to B and B to C distribute torsional strain over a controlled distance. (right) While torsionally unconstrained, the probe cable is isolated from moving parts on the mapper.

5.3.8 Alignment

Alignment between the mapper and a magnet under test is achieved through iterative fine tuning and measurement. Designed and fabricated by TRIUMF, a turnbuckle table provides six degree-of-freedom control over the mapper's position and rotation. As discussed in **Section 5.2.3**, rotational alignment is prioritized as it cannot be corrected in software.

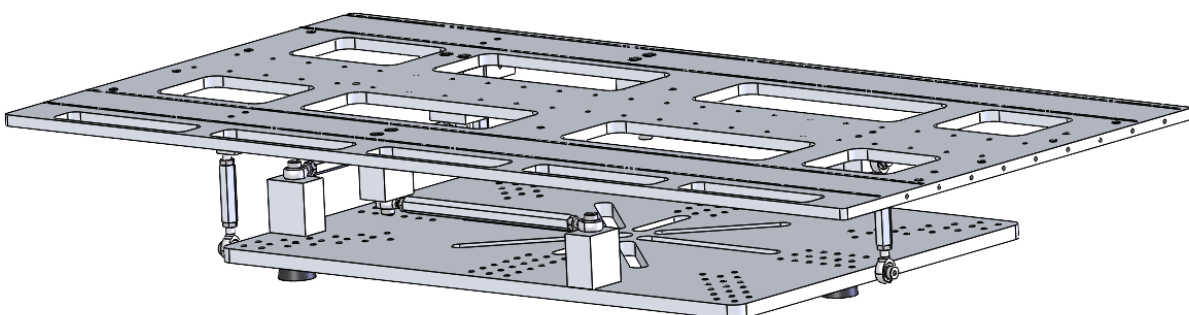


Figure 26. Turnbuckle alignment table. A detailed description of this style of alignment device is available in print (Thur et al., 1997).

The table did have some play due to play in the turnbuckles. This was addressed with the addition of a 7th turnbuckle.

Measurement at TRIUMF is performed by Coordinate Measuring Machines (CMMs) seen in

Figure 27. Retroreflective targets are included on the baseplate and the mapper for compatibility with the laser CMM.

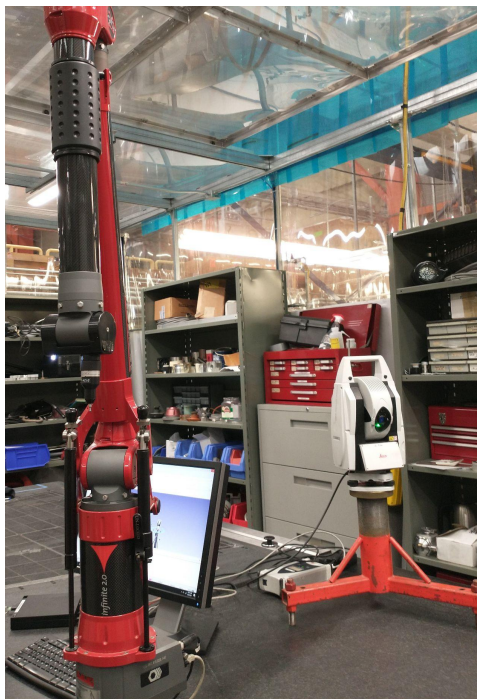


Figure 27. (left) Touch CMM used to measure surfaces with respect to each other. (right) Laser CMM used to track positions tagged with retro reflective targets. Both systems are capable of measurements with absolute accuracy on the order of 10 microns.

5.3.9 Probe Electrical Interface

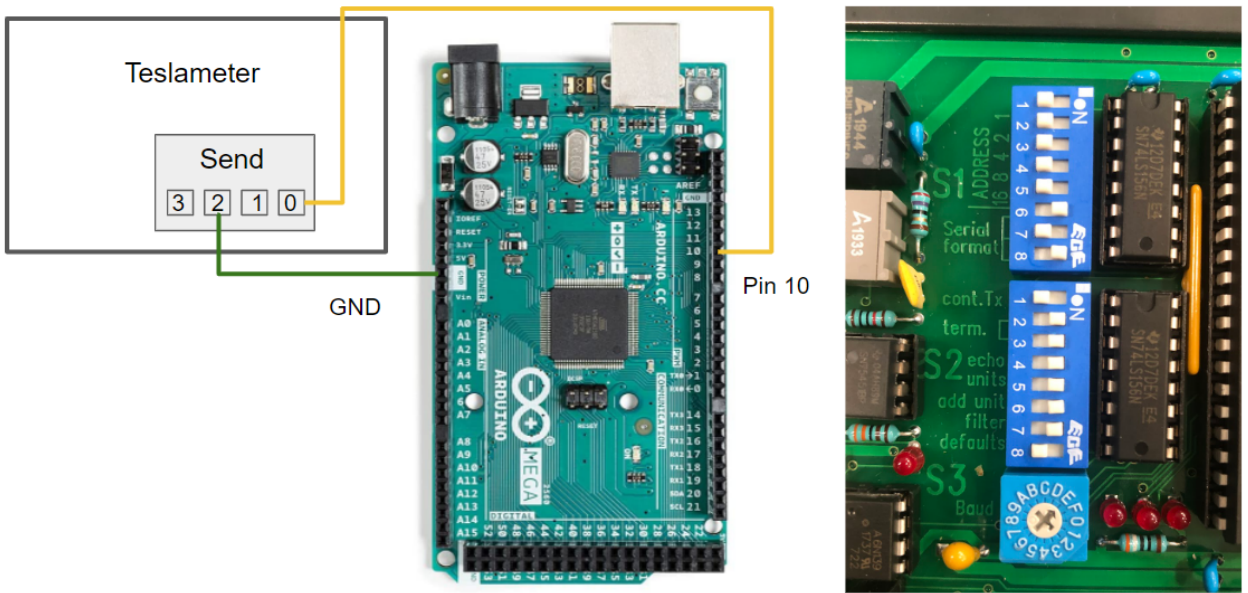


Figure 28. (left) Connection between Teslameter and board. (right) Teslameter switches to adjust serial settings.

The electrical interface contains an Arduino that reads the field data from the Teslameter and sends the decoded ASCII string via USB. The Teslameter switches are modified so the serial package contains eight data bits, no parity bit, and one end bit — the required frame for Arduino Software Serial port. Since TRIUMF has existing RS232 hardware installed on site, this is only a temporary solution for prototyping.

5.3.10 Software System

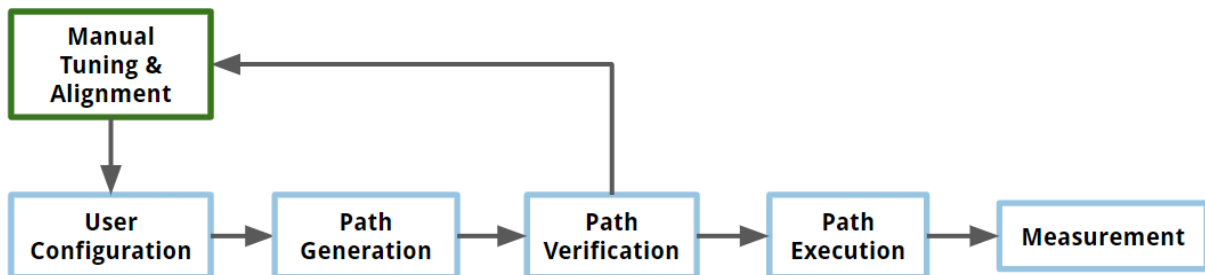


Figure 29. Software System Flowchart. Green boxes are completed by TRIUMF specialists and blue boxes implemented in our software.

TRIUMF specialists manually align the mapper using the existing Zaber control software. Our custom software contains five classes specialized to magnet mapping.

Alignment

TRIUMF specialists will manually align the stages using Zaber Launcher (see **Appendix 10.2**). They then record the position of the mapper when it is aligned with the center of the magnet. This position becomes the mapping origin.

User Configuration

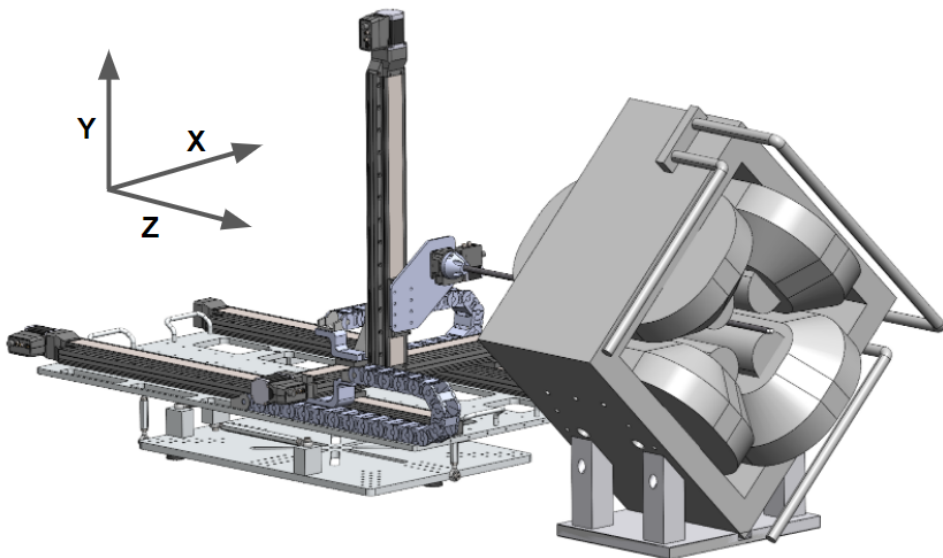


Figure 30. Mapper Coordinate System. Z is the direction parallel to the beam axis, X is the horizontal transverse direction, and Y is the vertical transverse direction.

```

1) path_filename = path/path.csv
2) path_edges_filename = path/path_edges.csv
3) data_filename = data/BL4N-STY1-00x12x80-0x2x2-220401-1330.csv
4) shape = rectangular
5) probe_stop_time_sec = 5.0
6) comm_port_zaber = COM3
7) comm_port_probe = COM4
8) x_range = 40
9) x_spacing = 20
10) y_range = 100
11) y_spacing = 20
12) z_range = 800
13) z_spacing = 20
14) x_offset = 250
15) y_offset = 250
16) z_offset = 500
17) x_accel = 25
18) y_accel = 25
19) z_accel = 25
20) rotation_points = [80.0]
21) collect_data = True
*****
Enter number of setting to edit, or 0 to exit: █

```

Figure 31. Terminal interface for setting configurations.

All configurations are stored in a JSON file. The user can change configurations by editing the JSON file directly, or via the command line interface.

TRIUMF's magnets can be covered by rectangular, cylindrical, and custom paths, each with different configurations. Appendix B contains detailed definitions and instructions for setting configurations.

Path Generation

The path is a 3D point cloud that fills the required mapping volume. Measurements are performed at all X, Y, Z positions at the same angle before rotation, as the rotational stage is slower than the linear stages.

Path Verification

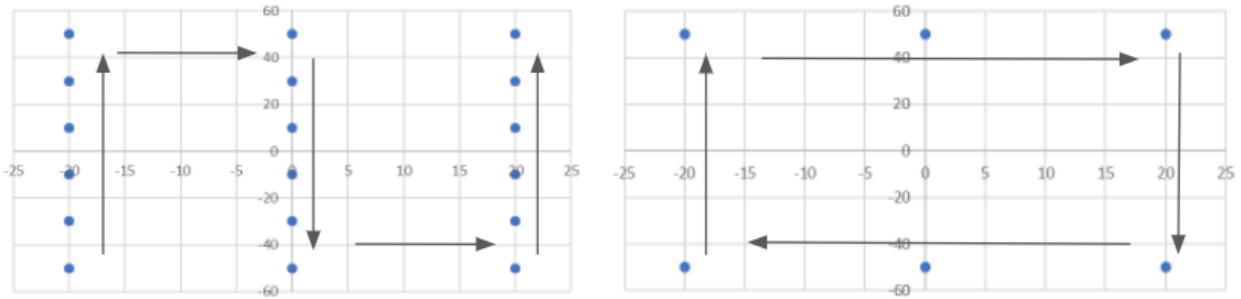


Figure 32. (left) Sample path in xy plane. (right) Sample path in xy plane for path verification.

The mapping software calculates the edges of the mapping path and runs the stages along the edges to ensure no collision occurs.

Measurement

The mapper measures the magnetic field at each point along the generated path, dropping any malformed data and recording multiple readings for redundancy. The output CSV file contains position, probe rotation, and field magnitude at each position.

5.4 Tests and Results

As we implemented our design, we performed a series of tests to characterize our system performance.

5.4.1 System Alignment

The stages were assembled at TRIUMF with the aid of CMMs to ensure the assembly was square. The 1 m passive rail, 1 m longitudinal linear stage, and horizontal stage are square to within 0.0038° , corresponding to an offset of 66 microns over the full range of motion. The worst alignment is in the vertical stage which is slanted at 0.04° from vertical with respect to the magnet mapper base in the longitudinal direction, corresponding to a 0.3 mm positional offset over the full range of motion. Further alignment information is included in **Appendix 9.5**.

We recommend placing shims between the vertical stage to horizontal issue to address this issue before mapping large volumes.

5.4.2 Boom Oscillation Testing

In **Section 5.3.4** we identified that oscillations of the boom could reduce system accuracy. The probe and its holder add additional mass to the boom, so we directly measured oscillations to determine the damping time.

We mounted an ADXL345 (SparkFun, n.d.) accelerometer to the tip of the boom, and recorded the response to motion system movement in each axis with different accelerations and distances. For this testing, the probe was mounted inside a boom with an unsupported length of 1.05 m. This is expected to be the longest boom used, so from the theory in **Section 5.3.4** these testing results form an upper bound on the required damping time.

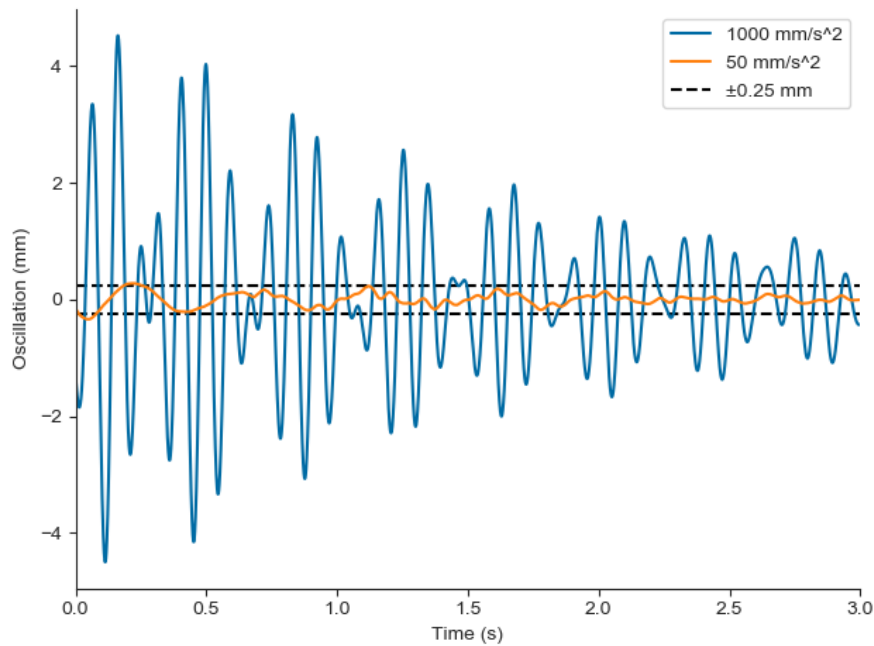


Figure 33. Processed accelerometer data of vertical (along gravity) boom oscillations during stage movement along the boom axis at different accelerations, with a maximum velocity of 100 mm/s. The vertical stage was located at its mid position for the high acceleration test, and at its highest extent for the low acceleration test. Data was collected on an ADXL345 accelerometer sampling at 3200 Hz at a range of ± 16 g. Repeated band pass filtering and integration was applied to extract the oscillating component of the displacement.

The motion system movement distance did not affect oscillation amplitude after movement, but the applied acceleration had a significant effect. Reducing the acceleration from 1000 mm/s^2 to 50 mm/s^2 ensured that boom oscillation during movement of all axes remained within 0.25 mm after 1 second.

In contrast to our expectations, we found that movement along the boom axis caused the most oscillation of the boom. Processed data for stage movement in this direction is shown in **Figure 33**. We noticed a beat frequency of approximately 2.5 Hz, which indicated that the boom oscillations were coupling with another close resonator in the system. **Figure 34** shows the acceleration spectral density, with two peaks close to 10 Hz. One is the reduced natural frequency of the boom due to the probe mass, and we suspect that the other is the natural frequency of the rotation to gantry bracket discussed in **Section 5.3.6**.

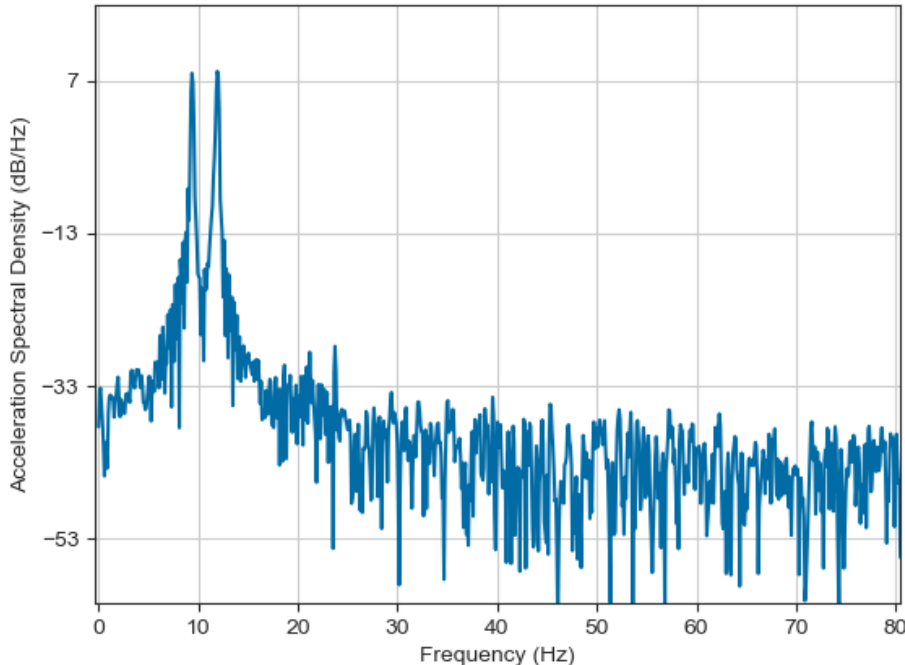


Figure 34. Section of the acceleration spectral density of the raw high acceleration discussed in Figure 35. Acceleration data was in m/s^2 and was sampled at 3200 Hz. Two peaks are visible at 11.9 Hz and 9.4 Hz.

To reduce oscillation during movement of the current mapper, the software system could be modified to reduce movement along the boom axis. Alternatively, the resonance frequency of the rotation to gantry bracket can be tested with the same accelerometer, and modifications can be made to raise its natural frequency and eliminate the coupling observed in these tests.

5.4.3 Magnetic Field Steerer Mapping



Figure 35. Field mapping test setup. The dashed box estimates the mapping region, which is a 2D rectangle with 120 mm in Y, 800 mm in Z direction, and 20 mm grid spacing. This mapping took 2.5 hours.

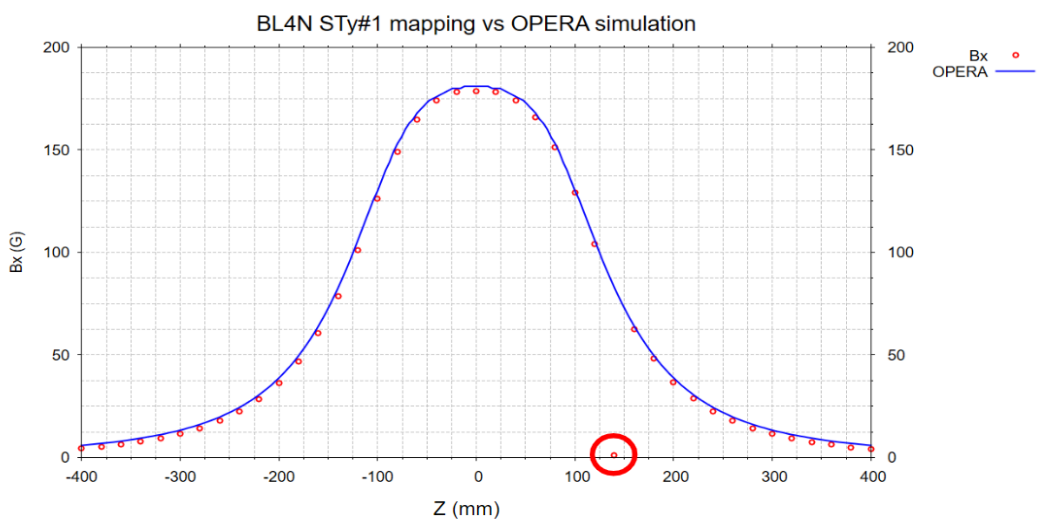


Figure 36. Magnet mapper magnetic field readings (red dots) in comparison to simulated field strength (blue line) as a function of longitudinal position. Outlier circled in red. These outliers occur sporadically due to incorrect readout from the probe. The data presented here was collected in 5 minutes.

To verify the mapper performance, TRIUMF set up a magnet with known field magnitudes and we performed a full mapping as shown in **Figure 36**. We allowed 5 s for the probe to settle within 0.1 Gauss and used 25 mm/s^2 acceleration to minimize boom oscillation.

This initial testing demonstrates our mapper's capabilities from alignment to moving linear stages and making measurements. The results match the simulated fields closely. However, we notice an outlier data point due to communication instability.

5.4.4 Quadrupole Magnet Mapping

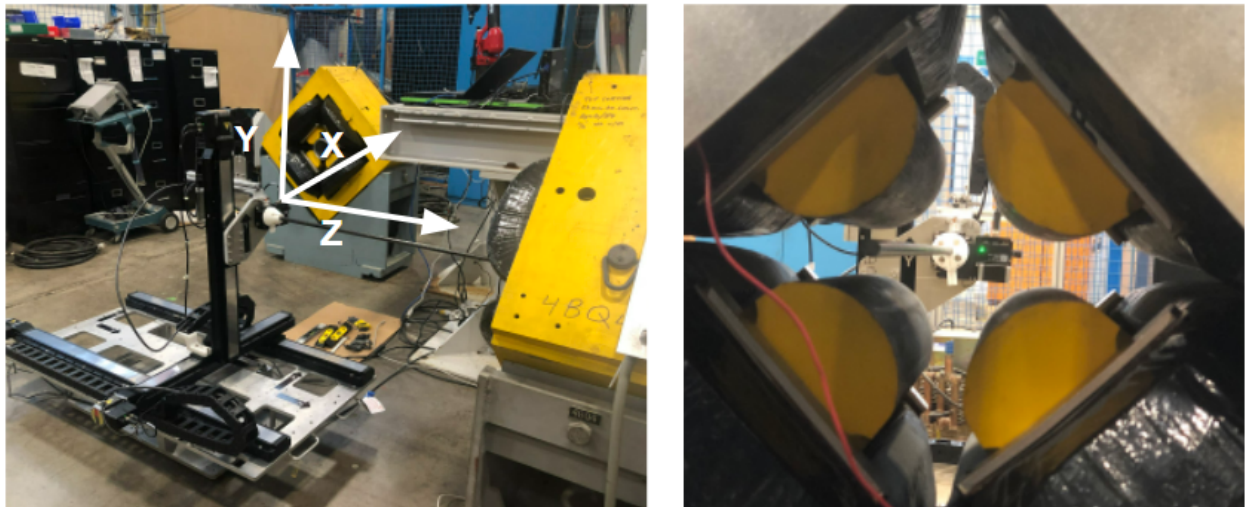


Figure 37. (left) Quadrupole magnet mapping setup (right) Side view with probe inside the magnet. The mapping region is a rectangular plane that is 100 mm in X direction with 5mm spacing, constant at 0 mm in Y, and 1000 mm in Z with 25 mm grid spacing. This mapping was completed in 2 hours.

We also mapped a quadrupole magnet under the same settling time and acceleration. This test aims to verify the accuracy of the motion systems in smaller regions and compatibility with larger fields.

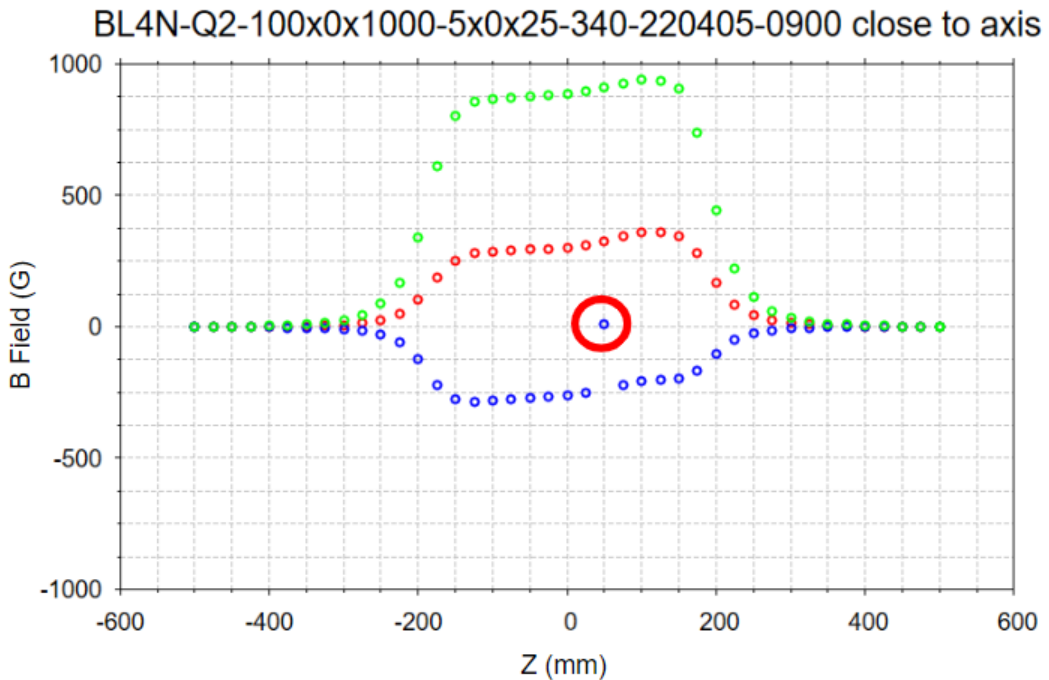


Figure 38. Quadrupole mapping results. The figure shows the magnetic field magnitude v.s. Z position at X = 0 mm, 5 mm, and -5 mm. Y = 0 for all series. Outlier data point circled in red.

After this mapping, we updated the regular expressions used for dataframe verification to better account for larger field magnitudes. However, outlier data points persist as a problem. We also noticed that along X=0, Y=0, the field is simulated to be nearly zero, but is measured to be more than 200 G near Z=0. TRIUMF determined that a misalignment between the boom axis and the rotation axis led to translational offset of around 5 mm as the probe was rotated. The misalignment must be addressed before we can produce relevant quadrupole data.

6 Conclusion

The overarching project goal was to deliver a magnet mapper immediately useful to TRIUMF. As seen in **Section 5.4.3** and **Section 5.4.4**, the mapper has already been used to map magnets but requires improvements before entering full-time service. We will examine our system's performance with respect to the main system requirements: measurement volume, timing, alignment, accuracy, magnetic interference, and budget.

The mapper can cover a mapping region of $0.5\text{ m} \times 0.5\text{ m} \times 1.0\text{ m}$, compatible with most magnets at TRIUMF. The motion system's expected accuracy is better than 0.25 mm, exceeding our 0.5 mm accuracy requirement to measure a 1mm grid spacing. We found accuracy is the main driver of a motion system's cost in comparison to measurement volume. However, the full system's actual accuracy is currently worse than the motion system's theoretical accuracy. The rotation system's axis misalignment (**Section 5.4.4**) and vertical stage's angular offset (**Section 5.4.1**) cause our current system accuracy to miss the 0.5 mm requirement by several mm. Both issues are addressed in **Section 7**.

With the chosen acceleration, 25 mm/s^2 , the boom oscillations are kept below 0.25 mm and traversing a 5mm grid step takes 0.9 seconds with less than 1 second of mechanical damping time. The selection of a high specific stiffness carbon fiber boom helps mitigate mechanical oscillation. The mapping time is dominated by the electronic damping time at 5 seconds. Mapping times have been a few hours during our tests; however, the timing will limit the mapping resolution that can be achieved in a reasonable time (**Figure 10**).

We have not seen any indications of magnetic interference from our initial tests; however, the stray magnetic fields produced by the mapper should be quantified to validate the system's measurements.

The full cost of the system components specified by our team was \$18,938 CAD, fitting to our sponsor's budget guideline. Additional costs (not included in the total above) related to this project include the turnbuckle table, hall probe, and teslameter.

Our testing (**Section 5.4.3**) revealed that magnet mapper data is sometimes lost from communication errors with the teslameter. As well, the mapper seemed to lose track of its position when left stationary overnight. These behaviours must be investigated further. We provide recommendations to address the outstanding issues in **Section 7**.

7 Recommendations

There are numerous improvements that could be made to improve the performance, reliability, and safety of the magnet mapper system. Our recommendations for improving the system are outlined below.

Boom Axis Alignment

In **Section 5.4.4**, we noted angular misalignment between the rotation stage and boom led to translational offsets as the probe was rotated. A new rotation stage to boom adapter has been produced by TRIUMF and is awaiting testing.

Vertical Stage Alignment

We noticed the vertical stage had some angular offset from vertical in the longitudinal direction. We recommend installing shims between the vertical and horizontal stages to remove the angular misalignment.

Packet Loss

Occasionally, the serial connection with the hall probe provides corrupted data. This can be fixed by reading the data 3 times and choosing the two data points that are closest to each other. It is generally obvious which datapoint is wrong since it differs by an order of magnitude.

Check for Drift

Should additional tests confirm that the mapper loses track of its position overtime, we recommend homing at regular intervals. Rotary encoders may also improve the system's ability to detect position drift.

Emergency Stop Button

Adding an easily recognizable emergency stop button will enable a safe shutdown as well as prevent any further damage to the system by cutting power to the Zaber stage motor controllers. The emergency stop must be approved by a TRIUMF electrician prior to installation.

Rotation Hardstop

One outstanding risk is that of damaging the probe cable if the rotation stage rotates too far. To safeguard against this, we recommend adding a physical hardstop to restrict the angle of the rotation stage. Currently we rely on the firmware's digital limits which have worked well so far, but adding a physical hardstop would further reduce this risk.

Integration With EPICS

To make operation and data collection easier, the system can be integrated with TRIUMF's system control software called EPICS. We kept our software system quite modular and parameterized to make future integration with EPICS simple with minimal software rewrite.

Reducing Mapping Time

If mapping time becomes an issue, a dense point cloud can be taken only near the expected beamline which is along the center axis of the magnet shown in blue in **Figure 8**. Then measurements can be taken more sparsely in the areas further from the expected beamline, shown in a transparent grey in **Figure 8**. As outlined in **Section 6**, a faster settling probe would greatly improve mapping time.

8 Deliverables

#	Description	Location
1	Complete System CAD Assembly	TRIUMF Deliverables Package\TMM0100-8.zip
2	Mapper Control Software	https://github.com/Alice-Xiong/magnet_mapper_control
3	Mapper Control Software Documentation	https://alice-xiong.github.io/magnet_mapper_control/
4	Boom Oscillation Data	TRIUMF Deliverables Package\Oscillation_Data.zip
5	Boom Oscillation Data Analysis Code	TRIUMF Deliverables Package\accelerometer_data_analysis_report.py
6	Project Proposal	TRIUMF Deliverables Package\2204 - 16T Magnet Mapper - Project Proposal
7	Project Presentation	TRIUMF Deliverables Package\2204 - 16 T Magnet Mapper - Presentation
8	Project Poster	TRIUMF Deliverables Package\2204 - 16 T Magnet Mapper - Poster

9 Appendix A

9.1 Bill of Materials

Item Name	Quantity	Unit Cost (\$ USD)	Source	Images
1 m driven stage (X-LRT1000BL-C)	1	3811	Zaber	-
0.5 m driven stage (X-LRT0500BL-C)	2	3333	Zaber	-
Rotation stage (X-RSW60A)	1	2170	Zaber	-
1 m passive stage (LRT1000G-CM00)	1	1530	Zaber	-
Motion system power supply (PS15S-48V65)	1	168	Zaber	-
Motion system angle bracket (AB151)	1	164	Zaber	-
USB to M8 adapter (X-USBDC)	1	44	Zaber	-
6' motion system data and power cable (X-DC06)	3	20	Zaber	-
6' carbon fiber boom (8069N13)	1	146.36	Zaber	-
Turnbuckle system and Baseplate	1	-	Waterjet and machined	
Gantry to rotation stage adapter plate	1	-	Waterjet	
Probe holder (top)	1	-	SLA 3D printed	
Probe holder (bottom)	1	-	SLA 3D printed	
Probe holder compliant	1	15.20	McMaster	-

rubber, 35A hardness (86435K15)				
1' of cable chains (4409T51)	8	21.49	McMaster	-
Cable chain end bracket (4556T82)	6	13.07	McMaster	-
Boom to rotation adapter	1	-	FDM 3D printed	
Top cable hold down	1	-	FDM 3D printed	
Bottom cable hold down	1	-	FDM 3D printed	
Rod attachment for strain relief	1	-	FDM 3D printed	
Cable retainer	1	-	FDM 3D printed	
2st stage cable chain mounting bracket	1	-	FDM 3D printed	
Top horizontal stage bracket	1	-	FDM 3D printed	
80/20 aluminum extrusion	1	-	Project Lab	-
Torsion relief bracket	1	-	Waterjet	

L bracket gantry to vertical cable chain	1	-	Hand machined	
L bracket rotation to extrusion	1	-	Hand machined	
Horizontal stage bracket	1	-	Waterjet	

9.2 Boom Optimization Calculations

The majority of the information in this section was drawn from Roark's Formulas for Stress and Strain (Budynas & Sadegh, 2020).

In this section, the following parameters are used:

$$\begin{aligned}
 E &= \text{Young's Modulus (Pa)} \\
 \rho &= \text{Density (kg/m}^3\text{)} \\
 g &= \text{Gravitational Acceleration (m/s}^2\text{)} \\
 l &= \text{Beam length (m)} \\
 w &= \text{Distributed Load (N/m)} \\
 W &= \text{Tip Load (N)} \\
 r_o &= \text{Outer Radius (m)} \\
 r_i &= \text{Inner Radius (m)} \\
 \zeta &= \text{Damping Ratio (Unitless)}
 \end{aligned}$$

We treated the boom as a simple harmonic oscillator, which means that the envelope of the oscillation amplitude is given by:

$$\text{envelope}(x(t)) = Ae^{-\zeta\omega_n t}$$

We want to decrease the time required for this envelope to decay. The damping will be essentially fixed and is difficult to predict, so this means the natural frequency must be maximized. For a cantilever beam with a distributed load (caused by its own weight) and a tip load (probe weight), the natural frequency in radians per second is given by:

$$\omega_1 \approx 1.732 \sqrt{\frac{EIg}{Wl^3 + 0.236wl^4}}$$

The second moment of area for an annulus, as needed for a hollow circular boom, is given by:

$$I = \frac{\pi}{4}(r_o^4 - r_i^4)$$

If the tip load and length is fixed, by substituting in the distributed load using the density of the material and the area of the cross section:

$$\omega \propto \sqrt{\frac{EI}{w}} = \sqrt{\frac{E\pi/4(r_o^4 - r_i^4)}{\rho\pi(r_o^2 - r_i^2)}} = \sqrt{\frac{E}{\rho}(r_o^2 + r_i^2)}$$

If the outer diameter is fixed, this means the ideal boom has a thin wall and a high Young's modulus divided by its density, often called the specific stiffness.

9.3 Hall Effect Sensors

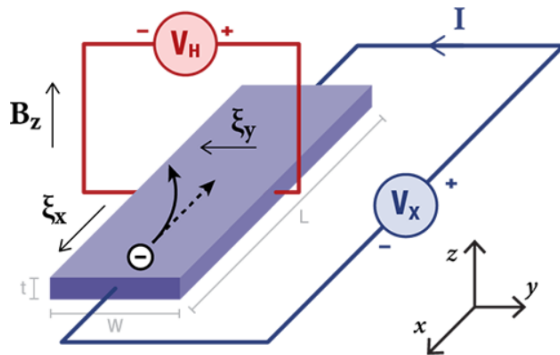


Figure 39. Hall Probe Diagram (Hall (Magnetic) Sensors, 2019).

Hall effect sensors are devices which can measure the strength of magnetic fields. The theoretical operation is as follows:

1. A magnetic field, B_z , is applied perpendicular to the sensing region (rectangle, left).
2. V_x is an externally applied voltage inducing current, I
3. As electrons traverse the sensing region, they interact with B_z and are deflected.
4. The deflected electrons generate a potential difference along ξ_y proportional to the applied field, B_z .
5. The potential V_H is measured, producing the magnetic field reading.

Notice that this measurement is only sensitive to magnetic fields perpendicular to the probe's sensing region.

Further descriptions of operation are available in literature (Ramsden Chapter 1, 2006).

9.4 Accuracy and Repeatability

Accuracy is the maximum difference between commanded and actual position over the full motion range, while repeatability is the maximum difference when the system is commanded to the same position multiple times.

This can be seen in **Figure 40**, where an imaginary motion system moving along the horizontal axis was commanded to the target position indicated by the blue line multiple times, but actually moved to the positions indicated by the red lines. Here accuracy is the maximum distance of the red lines from the blue, and repeatability is the spread of the red lines.

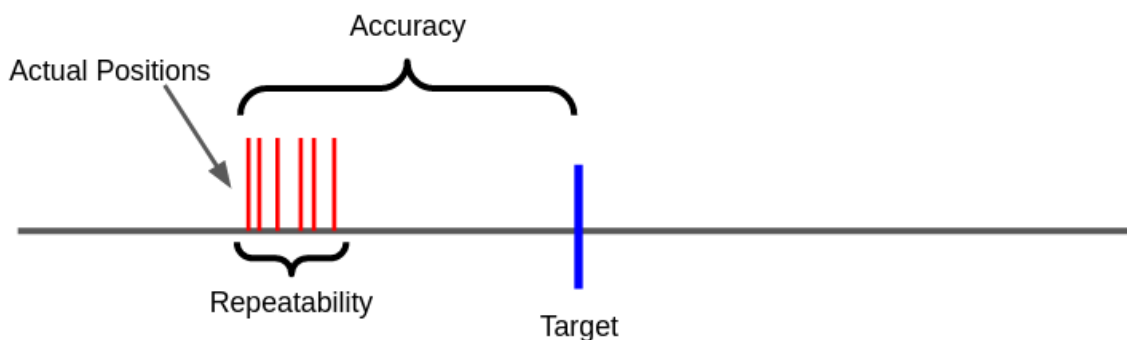


Figure 40. Visual representation of accuracy and repeatability.

In motion systems repeatability is often quite high, but achieving high accuracy generally requires precision machining and encoders for feedback. So generally accuracy drives the cost of a motion system.

9.5 System Alignment Report

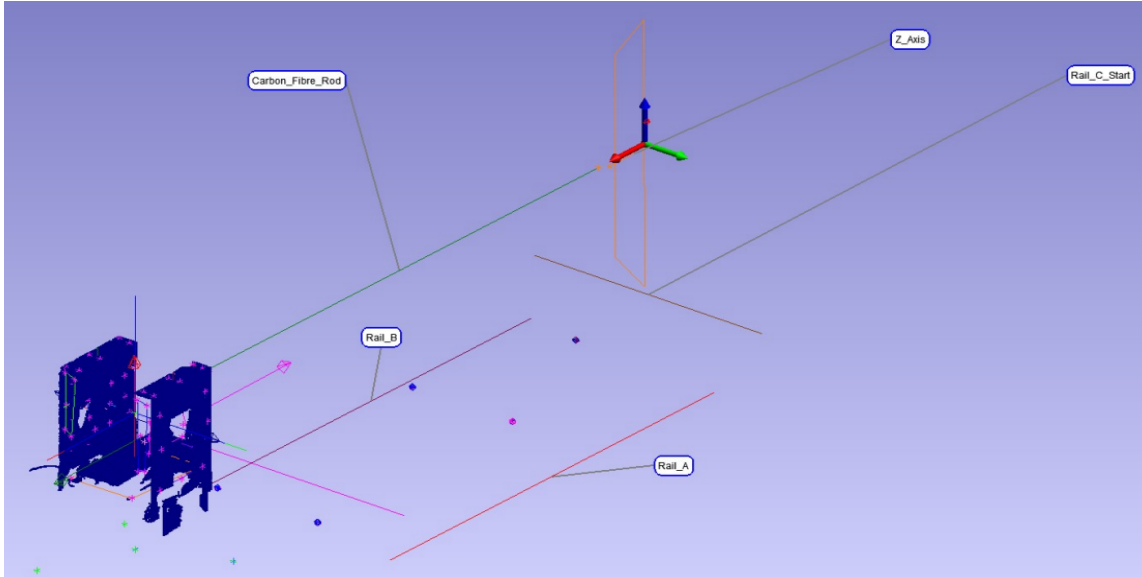


Figure 41. Alignment Report Axis Labels.

Object to Object Direction Relationship Direction: Rail_A to Rail_C_Start Reported in aligned_steerer::Frame_Probe_Base			Object to Object Direction Relationship Direction: Rail_B to Rail_C_Start Reported in aligned_steerer::Frame_Probe_Base		
	Angle (deg)	Distance (mm)		Angle (deg)	Distance (mm)
Angle Between Mutual Perp. Dist.	90.0003	89.9828	Angle Between Mutual Perp. Dist.	90.0035	89.9939
Proj. Ang. Difference			Proj. Ang. Difference		
Rx from Y	-90.0014		Rx from Y	127.0958	
Ry from Z	-102.2907		Ry from Z	77.7130	
Rz from X	-90.0003		Rz from X	90.0035	

Object to Object Direction Relationship Direction: Rail_A to Z_Axis Reported in aligned_steerer::Frame_Probe_Base			Object to Object Direction Relationship Direction: Rail_B to Z_Axis Reported in aligned_steerer::Frame_Probe_Base		
	Angle (deg)	Distance (mm)		Angle (deg)	Distance (mm)
Angle Between Mutual Perp. Dist.	0.0464	190.6648	Angle Between Mutual Perp. Dist.	179.9493	273.8196
Proj. Ang. Difference			Proj. Ang. Difference		
Rx from Y	8.2244		Rx from Y	-134.6784	
Ry from Z	0.0457		Ry from Z	-179.9506	
Rz from X	0.0079		Rz from X	-179.9884	

Object to Object Direction Relationship Direction: Rail_C_Start to Z_Axis Reported in aligned_steerer::Frame_Probe_Base		
	Angle (deg)	Distance (mm)
Angle Between Mutual Perp. Dist.	90.0082	303.5844
Proj. Ang. Difference		
Rx from Y	98.2258	
Ry from Z	102.3364	
Rz from X	90.0082	

These values are not relevant.
The axis of rotation is a function of the
positions measured to define the lines and planes

Figure 42. Alignment Report Results.

9.6 Motion System Comparison

The budget and accuracy requirements narrowed the Zaber solutions down to the LRT and LC40 systems shown in **Figure 43**.

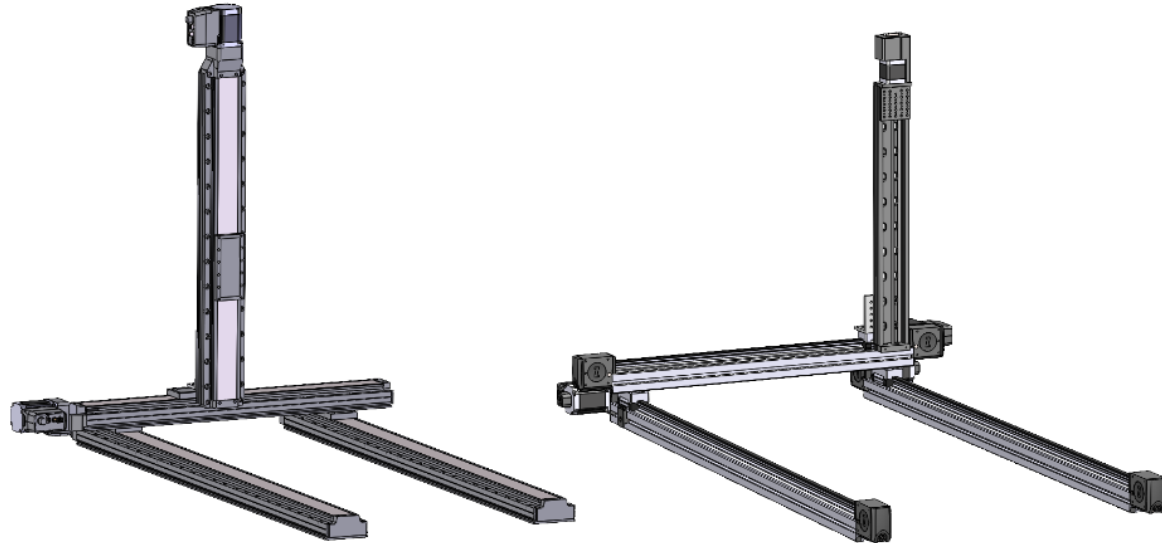


Figure 43. The LRT motion system (left) and the LC40 motion system (right).

The LRT option is made up of 3 leadscrew stages with high stiffness, load, and accuracy specifications, and includes a passive stage for support. The LC40 option uses 3 LC40 belt-driven stages, and a LSQ lead screw stage for the vertical axis.

We compared key parameters reported by Zaber and estimated by us to determine which option to recommend. These parameters are summarized in **Table 1**.

System Parameters	LRT	LC40
Linear Accuracy (mm)	0.25	0.93*
Repeatability (mm)	0.004	0.02
Angular Stiffness (Nm/ $^{\circ}$)	700	24
System Mass (kg)	28.3	12.3
Max Acceleration (m/s 2)	49	8.3
Cost (CAD\$)	15,335	11,249

Table 1. Comparison of motion system parameters for the LRT and LC40 systems. LC40 accuracy is starred (), as we were told its error is very linear and can be easily improved with a coordinate measurement machine, however the amount of possible improvement is uncertain.*

When talking with Zaber specialists, we were told that making exact predictions of motion system natural frequencies is difficult. We made a rough estimate of the comparative natural frequency between the two systems by assuming that the mass in each stage was similarly distributed, so that the difference in moment of inertia was only caused by a difference in overall stage mass. From the stage mass and stiffness specifications, we predicted that the LRT option would have a 4X higher natural frequency than the LC40. This is a significant benefit for oscillation reduction during system operation.

Due to the higher accuracy and estimated natural frequency, and because of the uncertainty in manual calibration of the LC40 system, we recommended the LRT option.

9.7 Mapper Assembly Views

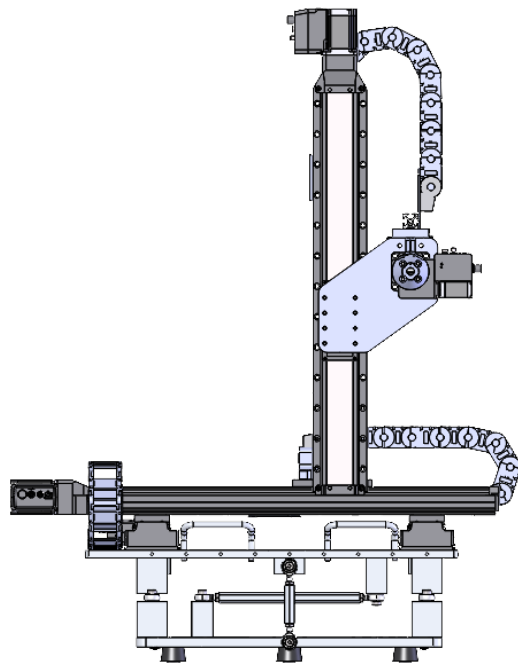


Figure 44. Mapper assembly front view.

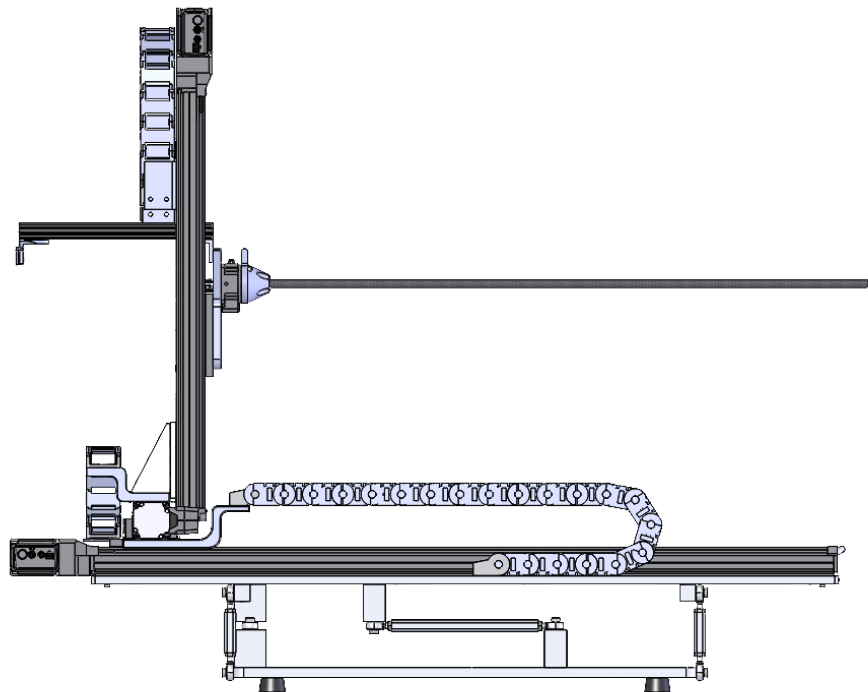


Figure 45. Mapper assembly side view.

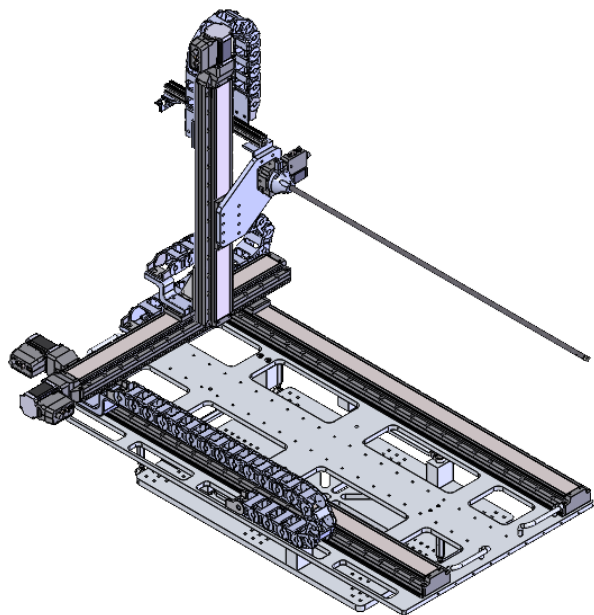


Figure 46. Mapper assembly isometric view.

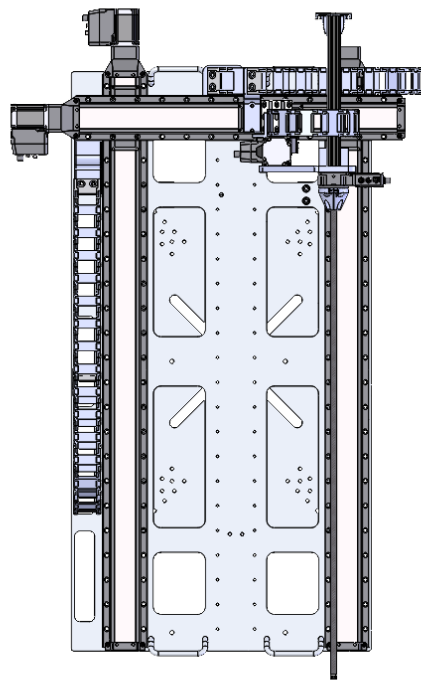


Figure 47. Mapper assembly top view.

9.8 Acknowledgements

Thank you to Dr. Marco Marchetto, Doug Preddy, Mike Vogel, and Mathew Brownell for proposing this project and for their support during the project.

Thank you to the Engineering Physics Project Lab staff, Dylan Gunn, Miti Isbasescu, and Bernhard Zender, for their tireless support.

Thank you to Michael McDonald and Mark Preddy at Zaber for their assistance selecting the motion system.

Thank you to the UBC Molecular Mechatronics Lab for providing SLA 3D printing service.

Thank you to Doug Sturgin at Group3 for his advice on hall probe measurement times.

10 Appendix B: User Manuals

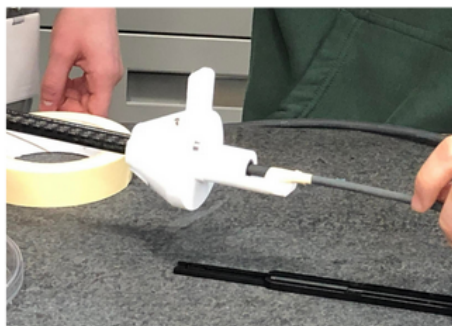
10.1 Probe Holder Installation



1) Remove probe from old holder



2) Cover probe head with heat shrink and tape the intersection



3) Feed probe + heat shrink through boom



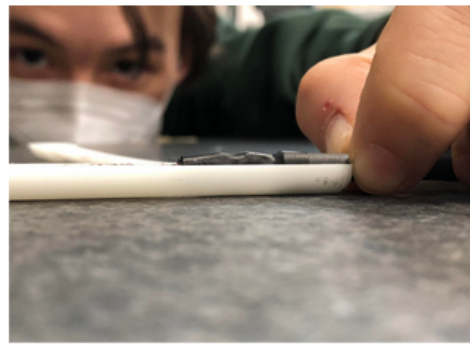
4) Gently push probe out on the other side



5) Remove tape and heat shrink, place probe on holder



7) Add the rubber sheet and top part of probe holder



6) Ensure unshielded cable is flush against probe holder



8) Push probe holder into boom

10.2 Zaber Launcher User Guide

Zaber Launcher is a graphical interface built by Zaber to allow manual control of the motion system and loading firmware configurations (*Zaber Software*, n.d.).

This section outlines how to use Zaber Launcher during manual alignment (**Section 5.3.10**) to move stages and record their position.

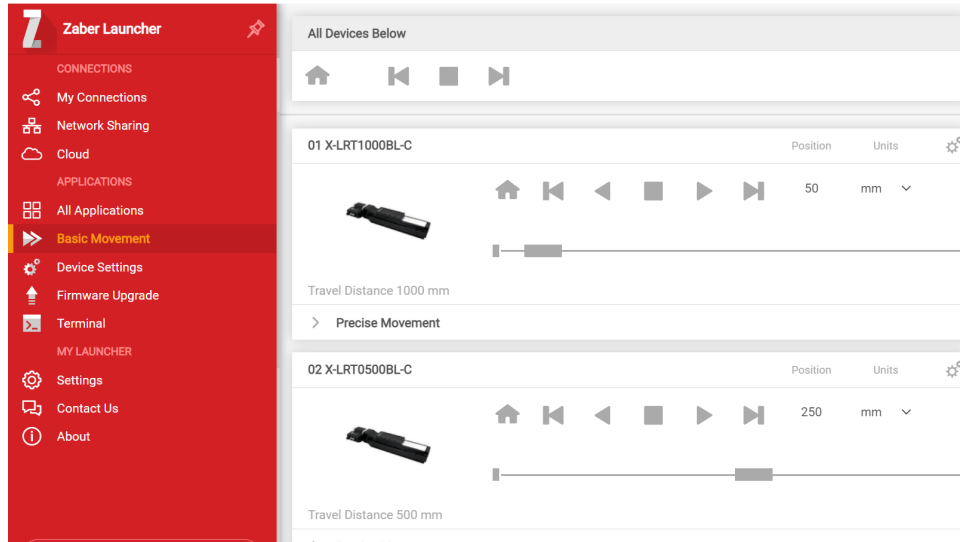


Figure 48. Basic movement window.

Open Zaber Launcher and select the basic movement tab on the left. The screen on the right will show the Zaber devices currently connected to this computer. Note that they are ordered according to their position in Daisy chaining:

- 1 — Z direction linear stage
- 2 — X direction linear stage
- 3 — Y direction linear stage
- 4 — Rotation stage

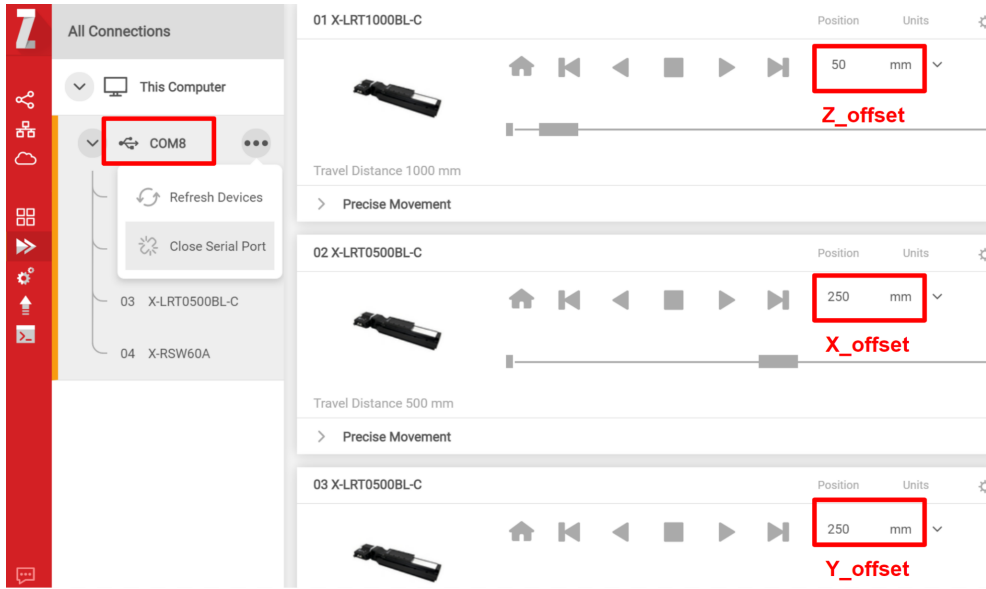


Figure 49. Checking the COMM port and X,Y,Z offsets in Zaber Launcher.

You can read the COMM port used by Zaber devices on the left tab and the current position of all devices are shown on the right side. The position of the stages should be entered into the mapper control software as the configurations X_offset, Y_offset, and Z_offset. ([Appendix 10.3](#))

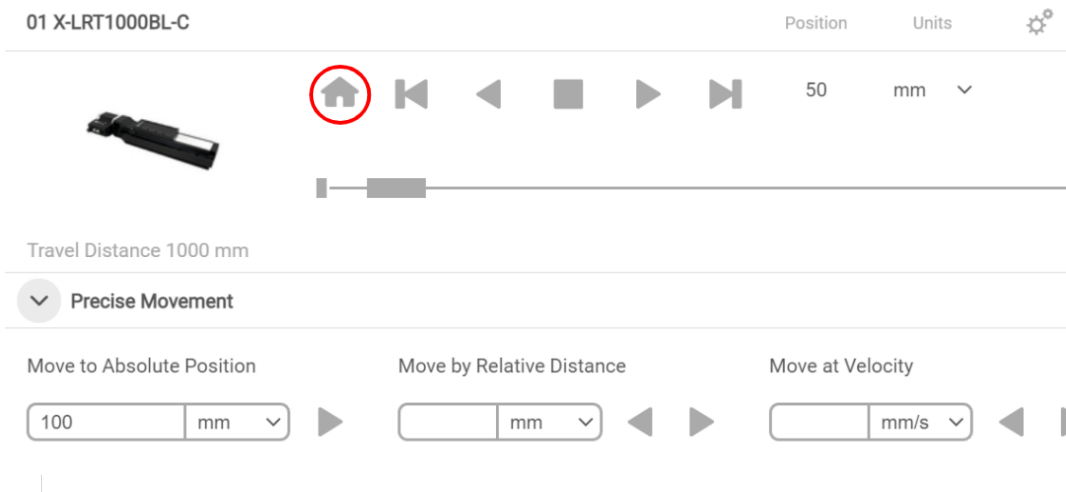


Figure 50. Moving the linear stages in Zaber Launcher.

Expanding the precise movement tab, you can move each stage by an absolute or relative distance. If you see the warning “WR”, it means the stage has not been homed. Homing can be done by clicking the house symbol, circled in red.



Figure 51. (left) Checking rotation and moving the rotation stage in Zaber Launcher. (right) Reference circle indicating the angles read at each position.

Motion and reading the position of the rotation stage is similar to that of linear stages. The user can manually rotate the stage using Zaber Launcher until they find the desired rotation angle. This angle is added to the configuration “rotation_angles” in the mapper control software. Note that the rotation stage rotates clockwise as shown on the reference circle.

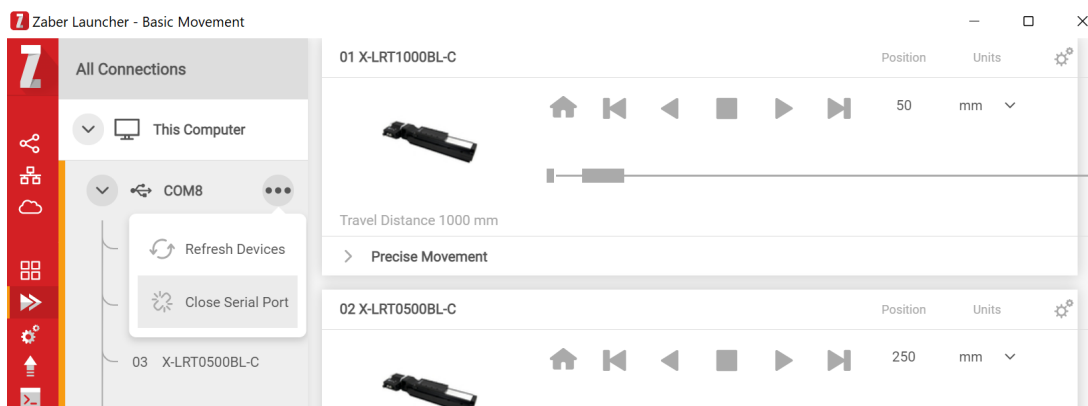


Figure 52. Close the serial port in Zaber Launcher.

To avoid interfering with the mapper control software, the user should close the serial port after using Zaber Launcher, as shown in **Figure 52**.

10.3 Mapper Control Software User Guide

This section outlines how to use the mapper control software. In particular, it emphasises how the user can change configurations in the user interface.

```
$ py main.py -c config_default.json -p custom  
Config file is config_default.json  
Profile name is custom
```

Figure 53. Starting the control software.

```
{ config.json > {} test_rectangular profile  
1 {"test_rectangular": [{"path_filename": "path/path.csv",  
2 "path_edges_filename": "path/path_edges.csv",  
3 "data_filename": "data/BL4N-Q2-100x0x1000-5x0x25-340-220404-1720.csv",  
4 "shape": "rectangular",  
5 "probe_stop_time_sec": 5.0,  
6 "comm_port_zaber": "COM3", |  
7 "comm_port_probe": "COM4",  
8 "collect_data": "True",  
9 "": ""}}
```

Figure 54. Identifying the profile in the configuration file.

The mapper control software can be downloaded via GitHub (link in **Section 8**), following the detailed installation instructions there. Open the folder that contains the software and run the above commands in any command line. Provide the name of the config file, usually “config.json” or “config_default.json”, to the “-c” argument. Provide the profile of the magnet to the “-p” argument. The profile is found in the config file, as shown in **Figure 54**.

If the user wishes to add a new profile, they can open “config_default.json”, copy the relevant profile, and paste it into “config.json”.

```

***** Main Menu *****

0) Change configurations
1) Generate path for mapping and for edges
2) Home the mapper
3) Run mapper along edges of mapping path
4) Start mapper in full mapping path

Press Q to exit the program

Enter the number of operation you would like to perform:

```

Figure 55. Main menu of mapper control software.

The program brings the user to a main menu with 5 options. The user can use enter 0 to change configuration. For a large number of changes, it may be faster to directly open the “config.json” file to edit configurations.

```

***** Current Mapper Settings *****
1) path_filename = path/path_cylinder.csv
2) path_edges_filename = path/path_cylinder_edges.csv
3) data_filename = data/data.csv
4) shape = cylinder
5) probe_stop_time_sec = 5.0
6) comm_port_zaber = COM10
7) comm_port_probe = COM1
8) collect_data = True
9) radius = 100
10) xy_spacing = 10
11) rotation_points = [0, 90]
12) z_range = 200
13) z_spacing = 10
14) x_offset = 100
15) y_offset = 250
16) z_offset = 250
17) x_accel = 25
18) y_accel = 25
19) z_accel = 25
*****
```

Path_filename: path to the CSV that stores the full mapping path

Path_edges_filename: path to the CSV that stores the mapping path boundaries

Data_filename: path to CSV that stores mapping data

Shape: Shape of path, can be cylinder, rectangular, custom

Probe_stop_time_sec: Time probe pauses at each spot

COMM_port_Zaber: COMM port that connects to Zaber device

COMM_port_probe: COMM port that connects to the probe

Collect_data: True if probe is installed, False if you do not want to collect any data

Figure 56. Configurations common to all motion shapes (I).

```
***** Current Mapper Settings *****
1) path_filename = path/path_cylinder.csv
2) path_edges_filename = path/path_cylinder_edges.csv
3) data_filename = data/data.csv
4) shape = cylinder
5) probe_stop_time_sec = 5.0
6) comm_port_zaber = COM10
7) comm_port_probe = COM1
8) collect_data = True
9) radius = 100
10) xy_spacing = 10
11) rotation_points = [0., 90]
12) z_range = 200
13) z_spacing = 10
14) x_offset = 100
15) y_offset = 250
16) z_offset = 250
17) x_accel = 25
18) y_accel = 25
19) z_accel = 25
```

Z_range: edge to edge distance in Z direction in mm. (-200, 200) correspond to z_range of 400.

Z_spacing: grid spacing of points in Z direction in mm.

X_offset (Y_offset, Z_offset): the position of stages when the tip of the probe is aligned to center of magnet in mm. This is read from Zaber Launcher.

X_accel (Y_accel, Z_accel): maximum acceleration in X, Y, Z directions in mm/s^2

Figure 57. Configurations common to all motion shapes (II).

The profiles are characterized by their “shape” attribute. There are three shapes:

- “Rectangular”: corresponds to a rectangular prism path
- “Cylinder”: corresponds to a cylindrical path with its side along the Z direction
- “Custom”: correspond to any custom path in X, Y, and rotation directions, that is repeated along the Z direction

Some configurations are common to all three shapes, including names of files, COMM port, probe settling time, and whether or not to collect data. Detailed description of the configurations are on **Figure 56 and 57**.

```
1) path_filename = path/path_cylinder.csv
2) path_edges_filename = path/path_cylinder_edges.csv
3) data_filename = data/data.csv
4) shape = rectangular
5) probe_stop_time_sec = 5.0
6) comm_port_zaber = COM3
7) comm_port_probe = COM4
8) collect_data = True
9) x_range = 100
10) x_spacing = 10
11) y_range = 100
12) y_spacing = 10
13) rotation_points = [80.0]
14) z_range = 100
15) z_spacing = 10
16) x_offset = 500
17) y_offset = 250
18) z_offset = 250
19) x_accel = 25
20) y_accel = 25
21) z_accel = 25
```

X_range , Y_range: edge to edge distance in X,Y direction in mm. (-100, 100) correspond to X_range, Y_range of 200.

X_spacing, Y_spacing: grid spacing of points in X, Y direction in mm

Rotation_points: a list of angles the probe will rotate to, in degrees

Figure 58. Configurations specific to rectangular motion shape.

```
***** Current Mapper Settings *****
1) path_filename = path/path_cylinder.csv
2) path_edges_filename = path/path_cylinder_edges.csv
3) data_filename = data/data.csv
4) shape = cylinder
5) probe_stop_time_sec = 5.0
6) comm_port_zaber = COM10
7) comm_port_probe = COM1
8) collect_data = True
9) radius = 100
10) xy_spacing = 10
11) rotation_points = [0, 90]
12) z_range = 200
13) z_spacing = 10
14) x_offset = 100
15) y_offset = 250
16) z_offset = 250
17) x_accel = 25
18) y_accel = 25
19) z_accel = 25
```

Radius: radius of circle in XY plane in mm.

XY_spacing: grid spacing of points in XY plane in mm.

Rotation_points: a list of angles the probe will rotate to, in degrees.

Figure 59. Configurations specific to cylinder motion shape.

```
***** Current Mapper Settings *****
1) path_filename = path/path_custom.csv
2) path_edges_filename = path/path_custom_edges.csv
3) data_filename = data/data.csv
4) shape = custom
5) probe_stop_time_sec = 5.0
6) comm_port_zaber = COM3
7) comm_port_probe = COM4
8) collect_data = True
9) custom_xyr_path_filename = path/path_xyr_custom.csv
10) z_range = 100
11) z_spacing = 100
12) x_offset = 500
13) y_offset = 250
14) z_offset = 250
15) x_accel = 25
16) y_accel = 25
17) z_accel = 25
```

Custom_xyr_path_filename: path to your custom path that specifies points in X, Y, and rotation. Units: mm for X,Y and degrees for rotation.

Figure 60. Configurations specific to custom motion shape.

There are also configurations specific to each magnet shape. They are outlined in **Figures 58, 59, and 60**. For rectangular and cylinder shapes, the user should note that values like “X_range” are given as point to point values. For example, measuring from -200 mm to 200 mm corresponds to an “X_range” of 400 mm.

```
Enter number of setting to edit, or 0 to exit: 10
Enter a new integer value for z_range, currently 100: 200
```

Figure 61. Changing the ‘z_range’ configuration.

To change any specific configuration, enter the associated number. For example, input 10 and press enter to change “z_range” on **Figure 61**. The user will then be prompted to enter a new value for that field. Input 200 and press enter to confirm. This will bring the user back to the configuration list, where they can select another config to change.

```
Enter number of setting to edit, or 0 to exit: 0

Do you want to save these settings? T to save to original file, N to save to a new file, any other key to save nothing. T

Setting now updated. Ready to rewrite path CSV? True (T) to start CSV writing, Q uit (Q) to exit the program, and press any key to go back to settings. T

***** Path generated according to custom XYR path *****

The current mapping sequence will take approximately 2.2 minutes.

***** Path for moving around edges generated *****

The current mapping sequence will take approximately 44.0 seconds.

***** Path for moving around edges generated *****
```

Figure 62. Confirming settings, saving, and generating path CSV.

After changing all configurations, enter 0 to exit and save the settings. If the user chooses to write to CSVs, two files will be generated:

1. CSV with points corresponding to the full mapping path
2. CSV with points corresponding to the edges of mapping path

The estimated time associated with these paths will also be generated.

```
***** Main Menu *****

0) Change configurations
1) Generate path for mapping and for edges
2) Home the mapper
3) Run mapper along edges of mapping path
4) Start mapper in full mapping path

Press Q to exit the program

Enter the number of operation you would like to perform:
```

Figure 63. Main menu of mapper control software.

After changing configurations, the user is brought back to the main menu. The other four functions can be accessed by entering the associated number:

1. The path for mapping and for edges is automatically generated if the user changes configuration within the mapper control software. If configurations are changed in the JSON file, then this option needs to run.
2. Homing the mapper is required before any motion occurs. We recommend homing the mapper after it has been idle for a long time to avoid drift and improve positional accuracy (**Section 7**).
3. Start moving the mapper along the points corresponding to the edges of the mapping path. Ensure Zaber COM port is set correctly and is not occupied by other software such as Zaber Launcher. Ensure all wires and obstacles are cleared before starting. We recommend running this option (3) before the full mapping (4) to ensure no collision.
4. Start the mapper in its full mapping path. The probe must be plugged in and powered. The Arduino interface must be connected to the COM port as configured to take data.

11 References

References

- Aguas, J. (2018). *MPT-141-2S, Hall Effect Probe, 2 meters | group3*. Group3. Retrieved April 3, 2022, from
<https://www.group3technology.com/product-page/mpt-141-2s-hall-effect-probe-2-meters>
- ARIEL begins a new future in rare isotopes – CERN Courier.* (2015, January 27). CERN Courier. Retrieved April 3, 2022, from
<https://cerncourier.com/a/ariel-begins-a-new-future-in-rare-isotopes/>
- Budynas, R. G., & Sadegh, A. M. (2020). *Roark's Formulas for Stress and Strain, 9E*. McGraw-Hill Education.
- Electromagnets.* (n.d.). ECE Northeastern. Retrieved April 4, 2022, from
<https://ece.northeastern.edu/fac-ece/nian/mom/electromagnets.html>
- Hall (Magnetic) Sensors.* (2019). Lake Shore Cryotronics. Retrieved April 3, 2022, from
[https://www.lakeshore.com/products/categories/magnetic-products/hall-\(magnetic\)-sensors](https://www.lakeshore.com/products/categories/magnetic-products/hall-(magnetic)-sensors)
- How do Synchrotrons Work?* (1997). How do Synchrotrons Work? Retrieved April 3, 2022, from
<http://pd.chem.ucl.ac.uk/pdnn/inst2/work.htm>
- Magnetic multipoles.* (n.d.). Taking a closer look at LHC. Retrieved April 3, 2022, from
https://www.lhc-closer.es/taking_a_closer_look_at_lhc/0.magnetic_multipoles
- Marchetto, M. (2021). *TRIUMF Magnet Images* [Images of magnets presented by Dr. Marchetto during our initial meetings.]
- Moreno, S. (2017, January 20). *Daisy-chaining Data and Power to Reduce Cabling - Technical Article*. Zaber. Retrieved April 3, 2022, from
<https://www.zaber.com/articles/daisy-chaining-data-and-power-to-reduce-cabling>

Ramsden, E. (2006). *Hall-effect sensors : theory and applications* (E. Ramsden, Ed.). Elsevier Science.

SparkFun. (n.d.). *SparkFun Triple Axis Accelerometer Breakout - ADXL345 - SEN-09836*.

SparkFun Electronics. <https://www.sparkfun.com/products/9836>

Thur, W., De Marco, R., Baldock, B., & Rex, K. (1997, October). *Rigid, Adjustable Support of Aligned Elements Via Six Struts*. SLAC. Retrieved April 4, 2022, from

<https://www.slac.stanford.edu/econf/C971013/papers/045.PDF>

Zaber Software. (n.d.). Zaber. Retrieved April 10, 2022, from <https://www.zaber.com/software>